

Cancer burden is controlled by mural cell- β 3-integrin regulated crosstalk with tumor cells

Ping-Pui Wong^{1,2,3,12*}, José M. Muñoz-Félix^{3,12*}, Maruan Hijazi⁴, Hyojin Kim⁷, Stephen Robinson⁸, Beatriz de Luxan-Delgado³, Irene Rodriguez-Hernandez⁵, Oscar Maiques⁵, Ya-Ming Meng^{1,2}, Qiong Meng^{1,2}, Natalia Bodrug³, Matthew Scott Dukinfield³, Louise E. Reynolds³, George Elia³, Andrew Clear⁴, Catherine Harwood⁹, Yu Wang¹⁰, James J. Campbell¹⁰, Rajinder Singh¹⁰, Penglie Zhang¹⁰, Thomas J. Schall¹⁰, Kylie P. Matchett¹¹, Neil C. Henderson¹¹, Peter W. Szlosarek⁶, Sally A. Dreger³, Sally Smith³, J. Louise Jones³, John G. Gribben⁴, Pedro R. Cutillas⁴, Pascal Meier⁷, Victoria Sanz-Moreno⁵ and Kairbaan M. Hodivala-Dilke^{3,13*}

¹ Guangdong Provincial Key Laboratory of Malignant Tumor Epigenetics and Gene Regulation, Sun Yat-Sen Memorial Hospital, Sun Yat-Sen University, Guangzhou, China 510120.

² Medical Research Center, Sun Yat-Sen Memorial Hospital, Sun Yat-Sen University, Guangzhou, China 510120.

³Centre for Tumor Biology,

⁴Centre for Haemato-Oncology,

⁵Centre for Tumour Microenvironment

⁶Centre for Molecular Oncology

Barts Cancer Institute – a CR-UK Centre of Excellence,

Queen Mary University of London,

John Vane Science Centre,

Charterhouse Square,

London,

EC1M 6BQ,

United Kingdom.

⁷The Breast Cancer Now Toby Robins Research Centre,

Institute of Cancer Research,

Mary-Jean Mitchell Green Building,

Chester Beatty Laboratories,

237 Fulham Road,

London SW3 6JB, UK.

⁸Gut Microbes and Health,

Quadram Institute Bioscience,

Norwich Research Park,

Norwich, UK, NR4 7UQ. And
School of Biological Sciences,
University of East Anglia,
Norwich Research Park,
Norwich, UK,
NR4 7TJ.

⁹Centre for Cell Biology and Cutaneous Research,
Blizard Institute,
Barts and The London School of Medicine and Dentistry,
Queen Mary University of London,
London,
E1 2AT,
United Kingdom.

¹⁰ChemoCentryx Inc.
850 Maude Ave, Mountain View
CA94043
USA.

¹¹Centre for Inflammation Research, The Queen's Medical Research Institute, Edinburgh
BioQuarter, University of Edinburgh, Edinburgh, UK.

¹²These authors contributed equally to this MS.

¹³ Lead contact.

*Corresponding authors:

k.hodivala-dilke@qmul.ac.uk (K.H.-D.),
huangbp3@mail.sysu.edu.cn (P.-P.W.),
j.munoz-felix@qmul.ac.uk (J. M.-F.)

Keywords: mural-cell, β 3-integrin, paracrine

Running title: Mural-cell- β 3-integrin regulation of tumor growth

SUMMARY

Enhanced blood vessel (BV) formation is thought to drive tumor growth through elevated nutrient delivery. However, this observation has overlooked potential roles for mural cells in directly affecting tumor growth independent of BV function. Here we provide clinical data correlating high percentages of mural- β 3-integrin negative tumor BVs with increased tumor sizes but with no effect on BV numbers. Mural- β 3-integrin loss also enhances tumor growth in implanted and autochthonous mouse tumor models with no detectable effects on BV numbers or function. At a molecular level, mural-cell β 3-integrin loss enhances signalling via a FAK-p-HGFR-p-Akt-p-p65 thus driving CXCL1, CCL2 and TIMP-1 production. In particular mural cell derived CCL2 stimulates tumor cell MEK1-ERK1/2-ROCK2-dependent signaling and enhances tumor cell survival and tumor growth. Overall, our data indicate that mural cells can control tumor growth via paracrine signals regulated by β 3-integrin, providing a previously unrecognised mechanism of cancer growth control.

HIGHLIGHT

- High percentages of mural- β 3-integrin negative tumor BVs associate with poor prognosis in human cancers
- Mural- β 3-integrin loss enhances tumor growth in implanted and autochthonous mouse tumor models without affecting BV numbers.
- Mural- β 3-integrin loss upregulates FAK-p-HGFR-p-Akt-p-p65 driven CXCL1, CCL2 and TIMP-1 production.
- Mural cell derived CCL2 activates MEK1-ERK1/2-ROCK2-dependent tumor cell survival and tumor growth.

IN BRIEF

Weak mural- β 3-integrin expression associates strongly with poor prognosis in multiple cancers. Depletion of mural- β 3-integrin stimulates cytokine production via the upregulation of FAK-p-HGFR-p-Akt-p-p65 signaling. Mural cell derived CCL2 activates tumor cell growth via MEK1-ERK1/2-ROCK2 pathway. 'Pericrine' signalling, ie. Pericyte derived signals can directly regulate tumor cell growth without affecting blood vessel function.

INTRODUCTION

The precise mechanisms underlying the role of tumor stromal cells in cancer growth are still unclear. In solid cancers, blood vessels are essential for the delivery of nutrients and oxygen (Hanahan and Weinberg, 2011). The formation of new tumor blood vessels, tumor angiogenesis, involves the enhanced proliferation and migration of endothelial cells, development of a vessel basement membrane and subsequent recruitment of supporting mural cells including pericytes (Chung et al., 2010). These cellular processes are thought to require changes in cell adhesion. The cell adhesion receptor, integrin $\alpha_v\beta_3$, is upregulated in nascent tumor blood vessels, in both endothelial cells and pericytes, suggesting a functional role for this integrin in tumor angiogenesis. Importantly, despite strong preclinical data and the fact that potent β_3 -integrin inhibitors are now under development, previous strategies to target β_3 -integrin as anti-angiogenic and anti-cancer strategies have failed in clinical trials (Mason, 2015; Tucci et al., 2014). This is most likely because a deeper understanding of the role of this integrin in tumor blood vessels and tumor biology is still required. Although β_3 -integrin in endothelial cells has been studied extensively (Brooks et al., 1994a; Brooks et al., 1994b; Brooks et al., 1995; Reynolds et al., 2009; Reynolds et al., 2002; Steri et al., 2014; Stupp and Ruegg, 2007), its role in pericytes still remains unknown.

Pericytes are generally recognised for being able to cross-talk with endothelial cells and regulate blood vessel leakage (Armulik et al., 2011; Raza et al., 2010; Stratman et al., 2009). However, the correlation of pericyte abundance in controlling cancer growth and progression is still unclear (Caspani et al., 2014; Cooke et al., 2012; Furuhashi et al., 2004; O'Keeffe et al., 2008; Sinha et al., 2016). Indeed, the molecular mechanisms behind the regulation of tumor progression by pericytes are still largely unknown. Recent studies have revealed that tumor endothelial cells can produce angiocrine factors, endothelial-derived factors, that can regulate tumor growth and chemosensitivity (Acharyya et al., 2012; Brantley-Sieders et al., 2011; Cao et al., 2014; Cao et al., 2017; Ghajar et al., 2013; Ghiabi et al., 2014; Gilbert and Hemann, 2010; Lu et al., 2013; Pedrosa et al., 2015; Tavora et al., 2014; Wieland et al., 2017). For example, NF- κ B signaling and its control of endothelial cell-derived cytokine production has been implicated in cancer progression and chemosensitivity (Acharyya et al., 2012; Cao et al., 2014; Cao et al., 2017; Gilbert and Hemann, 2010; Tavora et al., 2014). Similar roles for paracrine signals derived from pericytes were hitherto not known.

Our findings suggest a new concept whereby direct cross-talk between mural cells and tumor cells promote cancer growth and that this is controlled by mural cell- β_3 -integrin.

RESULTS

In human cancers high percentages of tumor blood vessels that are mural-β3-integrin negative correlate with increased tumor size and enhanced disease progression

Here we show that mural cell-β3-integrin was expressed only in a sub-set of blood vessels and that mural-β3-integrin-negative blood vessels were evident. The range of percentages of blood vessels that were mural-β3-integrin negative across individual patient samples was wide in human cutaneous melanoma (mean value 41%), diffuse large B cell lymphoma (mean value 49%) and ER+ breast cancer (mean value 57%) (**Figure 1 A; Supplementary figure 1 A-D**). A high percentage of mural-β3-integrin negative blood vessels (ie when more than the mean number of tumor blood vessels are mural-β3-integrin negative) correlated significantly with patients stratified into those with increased: (1) tumor burden in human cutaneous melanoma (identified by increased Breslow thickness); (2) tumor cell proliferation in human cutaneous melanoma (**Figure 1 B; Supplementary figure 1 E**); (3) tumor size in human diffuse large B cell lymphoma and human ER+ breast cancer (**Figure 1 B**), but not with a change in blood vessel density (**Figure 1 C**). Importantly, a high proportion of mural-β3-integrin negative blood vessels correlated with patients with: (1) elevated metastasis incidence (**Figure 1 D**); (2) increased disease progression stage (**Figure 1 E**); (3) elevated incidence of relapse (**Figure 1 F**) and (4) advanced aggressive cancer phenotype (**Figure 1 G**) in primary human cutaneous melanoma, diffuse large B cell lymphoma, ER+ breast cancer and mesothelioma respectively. Together these clinical data indicate that a high percentage of blood vessels that are mural-β3-integrin negative correlate with enhanced tumor size and progression, with no apparent effect on blood vessel density.

Generation and characterisation of *pdgfrβcre+;β3^{fl/fl}* mice

In order to elucidate the possible mechanisms by which pericyte-β3-integrin loss could regulate cancer growth and progression, we generated a mouse model of *pdgfrβcre*-driven-β3-integrin deficiency, where β3-integrin deficiency was confirmed in tumor pericytes. Mendelian ratios, male : female ratios and average mouse weights were all normal for mice born to *pdgfrβcre-;β3^{fl/fl}* × *pdgfrβcre+;β3^{fl/fl}* mice (**Supplementary figure 2 A-D**). *Pdgfrβcre+;β3^{fl/fl}* mice showed no apparent defects in non-tumor burdened tissues (**Supplementary figure 2 E**) with poor cre-activity in pericytes of unchallenged skin but good cre activity in tumour pericytes (**Supplementary Figure 2 F**) (Reynolds et al., 2017). Mural cell purity was established and cell survival was not affected by loss of β3-integrin (**Supplementary figure 2 H**). Loss of β3-integrin, but not β1 or β5 subunits, was evident only in pericytes isolated from *pdgfrβcre+;β3^{fl/fl}* mice (**Supplementary figure 2 I**). Pericyte specificity of deletion was supported by expression of β3-integrin in endothelial cells and fibroblasts from *pdgfrβcre+;β3^{fl/fl}* mice (**Supplementary figure 2 J and K**). These data indicate good specificity of β3-integrin deletion in tumor associated pericytes from *pdgfrβcre+;β3^{fl/fl}* mice in the systems tested.

Loss of pericyte-β3-integrin enhances tumor growth in mice

To examine the effect of pericyte-β3-integrin loss on tumor growth, *pdgfrβcre⁻;β3^{fl/fl}* and *pdgfrβcre⁺;β3^{fl/fl}* mice were injected subcutaneously with syngeneic mouse melanoma B16F0 and Lewis lung carcinoma (LLC) cells. Immunofluorescence analysis confirmed reduced β3-integrin expression in PDGFRβ-positive and αSMA-positive tumor blood vessel pericytes only in *pdgfrβcre⁺;β3^{fl/fl}* mice (**Figure 2 A; Supplementary figure 2 L**). B16F0 tumor growth and tumor cell proliferation (Ki67) were enhanced significantly in *pdgfrβcre⁺;β3^{fl/fl}* mice (**Figure 2 B; Supplementary figure 2 M**). The increase in tumor growth was confirmed using LLC tumor cells in *pdgfrβcre⁺;β3^{fl/fl}* mice (**Figure 2 C**). In a second experimental setting, B16F10 or LLC cells were injected via the tail vein and lung tumor burden measured by microCT imaging. No differences in the number of CMTPIX-labelled tumor cells homing (2 h post tail vein injection) or seeding (48 h post injections) were observed between the lungs of each genotype (**Supplementary figure 2 N**). However, at 16 days post inoculation enhanced tumor burden was observed in the lungs of *pdgfrβcre⁺;β3^{fl/fl}* mice (**Figure 2 D and E**). This correlated with an increase in the number and size of B16F10 and LLC lung nodules in *pdgfrβcre⁺;β3^{fl/fl}* mice (**Figure 2 F and G**). Orthotopic growth of syngeneic mammary E0771 tumour cells was also enhanced in *pdgfrβcre⁺;β3^{fl/fl}* mice (**Figure 2 H**). However, although no difference in the number of spontaneous lung metastases was observed, the size of E0771 lung metastases was significantly increased in *pdgfrβcre⁺;β3^{fl/fl}* mice (**Supplementary figure 2 O**). Corroborating these results at 13 weeks of age spontaneous pancreatic tumor growth was significantly enhanced in *RIPTag-2⁺;pdgfrβcre⁺;β3^{fl/fl}* mice compared with *RIPTag-2⁺;pdgfrβcre⁻;β3^{fl/fl}* mice (**Figure 2 I**). Together these data indicate that loss of pericyte-β3-integrin does not affect tumor cell homing or seeding at distant sites but is sufficient to enhance tumor growth at primary and secondary sites.

Pericyte-β3-integrin deletion does not cause detectable changes in tumor blood vessel numbers or function

The effect of pericyte-β3-integrin loss on vascular properties was next examined. Blood vessel density, detected by immunostaining for endomucin, was not significantly different in B16F0, B16F10, LLC or E0771 tumors in *pdgfrβcre⁻;β3^{fl/fl}* and *pdgfrβcre⁺;β3^{fl/fl}* mice or spontaneous pancreatic tumors in *RIPTag-2⁺;pdgfrβcre⁺;β3^{fl/fl}* and *RIPTag-2⁺;pdgfrβcre⁻;β3^{fl/fl}* (**Figure 3 A and B; Supplementary figure 3 A - D**). The percentage of blood vessels lacking mural cells were not significantly changed between genotypes (**Figure 3 A and B; Supplementary figure 3 E and G**). No differences between the percentage of tumor blood vessels perfused (**Figure 3 C; Supplementary Figure 3 F**) and the percentage of tumor blood vessels with basement membrane collagen IV in *pdgfrβcre⁻;β3^{fl/fl}* or *pdgfrβcre⁺;β3^{fl/fl}* mice were detected (**Figure 3 D; Supplementary figure 3 H**). Blood vessel leakage, tumour hypoxia and blood flow, were also not changed between genotypes (**Figure 3 E, F; Supplementary figure 3 I, J**). Lastly,

unchallenged skin of *pdgfr β cre-;* β 3^{fl/fl} and *pdgfr β cre+;* β 3^{fl/fl} mice showed no difference in blood vessel density, pericyte coverage or vessel leakage (**Supplementary figure 3 K**) most likely because previous reports, and our own data, indicate that *pdgfr β* -promoter activity is low in mural cells of normal quiescent vessels (see Supplementary figure 2 F) (Heldin, 2013; Pietras et al., 2002; Wang et al., 2010). Together, these data suggest that the enhanced tumor growth in *pdgfr β cre+;* β 3^{fl/fl} mice is not associated with any apparent effect on tumor blood vessel number, maturation, perfusion or flow functions and led us to investigate whether a possible paracrine effect of β 3-null pericytes on tumor cells could affect tumor growth directly.

Deletion of mural cell- β 3-integrin increases tumor cell growth independent of effects on tumor blood vessels

In order to test the paracrine effect of β 3-null mural cells on tumor growth we developed experiments where wild type C57BL/6 mice were co-injected with tumor cells and either WT or β 3-null pericytes and the resulting tumors analysed. Subcutaneous co-injection of B16F0 with β 3-null pericytes (1:8) showed enhanced tumor growth compared with co-injection of WT pericytes with B16F0 cells (**Figure 4 A; Supplementary figure 4 A**). No differences in tumor blood vessel density or pericyte coverage were observed between these groups (**Figure 4 B**). In a second model, co-injection of B16F10 cells with β 3-null pericytes via the tail vein of wildtype C57BL/6 mice increased the number of B16F10 lung nodules and relative nodule size above that of WT pericytes at both 1:4 and 1:8 ratios (**Figure 4 C; Supplementary figure 4 B**). Using CMTPIX tagged pericytes the survival of WT and β 3-null pericytes, after injection in C57BL/6 mice, was not different *in vivo* (**Figure 4 D**) suggesting that changes in tumor burden were not affected by differential pericyte survival. Furthermore, blood vessel density and pericyte coverage of blood vessels were not altered (**Figure 4 E; Supplementary figure 4 C**). B16F0 cell invasion was similar when B16F0 cells were incubated with conditioned media from WT or β 3-null pericytes, suggesting that tumor cell invasion is not affected by paracrine signals generated from β 3-null pericytes (**Figure 4 F**). In a further model, although the number of spontaneous E0771 lung metastases were similar between groups, the size of metastases was elevated in mice which had been co-injected with β 3-null pericytes (**Figure 4 G; Supplementary figure 4 D**). *In vitro*, conditioned medium from β 3-null pericytes was able to significantly enhance tumor cell number indicating that a paracrine signal from pericytes that controlled malignant cell growth (**Figure 4 H**). These data, together with the evidence that tumor cell homing and seeding in the lungs is not affected by loss of pericyte- β 3-integrin, suggested that tumor growth, either at primary or secondary sites, were enhanced by the loss of pericyte- β 3-integrin, pointing towards a possible paracrine mechanism of pericyte-tumor cell cross-talk that is regulated by pericyte- β 3-integrin.

Increased FAK-p-HGFR-p-Akt-NF- κ B signaling and subsequent chemokine production in β 3-deficient pericytes enhances tumor cell ROCK2 signalling and tumor cell survival

Next, the molecular mechanisms underlying pericyte- β 3-integrin – tumor cell cross-talk were explored. Unbiased, proteomics analysis of WT and β 3-null pericytes identified increased expression of multiple candidates in β 3-null pericytes. These included focal adhesion kinase (FAK) a major known regulator of integrin signalling (Guan, 2010) (**Figure 5 A; Supplementary Figure 5 A**). *Proteome-Profiler* tyrosine kinase and receptor tyrosine kinase arrays identified that β 3-null pericytes also had significantly elevated levels of p-HGFR, p-Akt (S473) and p-Akt (T308) when compared with WT pericytes (**Figure 5 B**). The enhancement of Akt signalling was further supported by the increased expression of phospho-Akt1 (S122) and phospho-Akt1 (S129) in β 3-null pericytes (**Supplementary Figure 5A**). Previous studies have shown that elevated HGFR phosphorylation can activate Akt activity (Usatyuk et al., 2014), which has previously been recognised to regulate angiocrine signalling from endothelial cells (Guerrouahen et al., 2014). At a molecular level, Akt activity is also known to regulate NF- κ B-mediated signalling (Cheng et al., 2011; Dan et al., 2008). Western blot analysis confirmed that in addition to increased pHGFR expression, phosphorylation of both Akt (at S473) and the NF- κ B subunit p65 (at S536) levels were elevated in β 3-null pericytes (**Figure 5 C**). The upregulation of activated p65 was confirmed by increased nuclear localisation of p-p65 in β 3-null pericytes (**Supplementary figure 5 B**). Pharmacological inhibition of β 3-integrin using cilengitide (Mas-Moruno et al., 2010) in WT pericytes also enhanced the levels of phospho-HGFR, -Akt and -p65 (**Supplementary figure 5 C**). Activation of p65 has been associated with the upregulation of cytokine production (Poulos et al., 2016; Tavora et al., 2014). Here, β 3-null pericytes produced significantly elevated levels of cytokine-related factors including sICAM-1, IL-1ra, CXCL1, CCL2 and TIMP-1 when compared with WT pericytes (**Figure 5 D**). The clinical relevance for the enhanced levels of p-Akt and nuclear p65 were supported by the significant up-regulation of p-Akt (**Figure 5 E; Supplementary figure 5 D and E**) and nuclear p65 (**Figure 5 F**) in the mural cells of human cancers where more than the mean percentage of blood vessels were mural- β 3-integrin negative.

In intervention studies FAK-kinase inhibitor (PF573228) treatment, reduced the expression of pY397-FAK and also the levels of p-HGFR, p-Akt and p-p65 in β 3-null pericytes (**Figure 5 G**). Secondly, treatment with the HGFR inhibitor, PHA-665752, reduced HGFR phosphorylation, p-Akt and subsequent p-p65 levels in β 3-null pericytes (**Figure 5 H**). Thirdly, treatment with the Akt inhibitor, LY294002, reduced both p-Akt and p-p65 levels (**Figure 5 I**). Together these data demonstrate that the elevated p-HGFR levels observed in β 3-null pericytes lead to an increase in Akt-phosphorylation and subsequent p65-phosphorylation.

The functional relevance of the molecular changes in p-HGFR, p-Akt and p-p65 in β 3-null pericytes were then evaluated. CRISPR-Cas9 gene editing of Akt in β 3-null pericytes (β 3-null;Akt^{KO} PC) resulted in a reduction in the phosphorylation and expression of total Akt as well as a reduction in p-HGFR but not total HGFR (**Figure 6 A**). CRISPR-Cas9 ablation of HGFR

in $\beta 3$ -null pericytes ($\beta 3$ -null;HGFR^{KO} PC) showed a reduction in the expression total HGFR and p-HGFR as well as a reduction in p-Akt but not total Akt (**Figure 6 A**). Together these data indicate cross-regulation of p-Akt and p-HGFR in $\beta 3$ -null pericytes. Downstream of this Akt- or HGFR-deletion resulted in a reduction in downstream p-p65 (but not total p65), TIMP-1 and CCL2. Furthermore, exposure of B16F0 cells to conditioned medium from $\beta 3$ -null;Akt^{KO} or $\beta 3$ -null;HGFR^{KO} pericytes resulted in significantly reduced tumor cell survival when compared to B16F0 cells exposed to conditioned medium from Cas9-control transfected $\beta 3$ -null pericytes ($\beta 3$ -null;Cas9) (**Figure 6 B**). Although gene-edited pericytes showed similar cell survival levels as controls (**Supplementary figure 6 A**), co-injection of $\beta 3$ -null;Akt^{KO} pericytes with B16F0 cells reduced the enhanced tumor growth observed in mice co-injected with B16F0 and $\beta 3$ -null;Cas9 pericyte controls (**Figure 6 C**). Together these data indicate a functional role for pericyte Akt and HGFR in the enhanced tumor cell survival induced by the loss of pericyte- $\beta 3$ -integrin.

The functional consequence of inactivation of NF- κ B signaling in $\beta 3$ -null pericytes was next assessed in the rescue of pericyte cytokine production and tumor cell growth control. $\beta 3$ -null pericytes were transfected with the super-repressor, non-phosphorylatable mutant form of I κ -B α , I κ -B α SR, which has been reported to repress the NF- κ B pathway (Pikarsky et al., 2004). $\beta 3$ -null pericyte transfection with the I κ -B α SR was sufficient to reduce p-p65 levels back to WT pericyte levels (**Figure 6 D**) and significantly reduce expression levels of CXCL1, CCL2 and TIMP-1 (**Figure 6 E**) indicating that NF- κ B signaling was involved in the regulation of these secreted factors. Furthermore, exposure of tumor cells to conditioned medium from I κ -B α SR transfected $\beta 3$ -null pericytes reduced the enhanced survival of B16F0, B16F10 and LLC cells when compared with exposure to conditioned medium from mock-transfected $\beta 3$ -null pericytes (**Figure 6 F**). *In vivo*, subcutaneous co-injection of B16F10 cells with I κ -B α SR transfected $\beta 3$ -null pericytes into C57BL/6 mice significantly decreased the number of lung nodules and relative nodule size when compared with mice co-injected with B16F10 cells and mock-transfected $\beta 3$ -null pericytes (**Figure 6 G**). No change in cell survival was observed between mock transfected or I κ -B α SR transfected $\beta 3$ -null pericytes (**Supplementary Figure 6 B**) suggesting that altered cell survival was unlikely to be responsible for the altered tumor growth in Figure 6 G. Together these data indicate that the functional role of NF- κ B signalling in $\beta 3$ -null pericyte control of tumor growth.

To test the functional relevance of the enhanced levels of $\beta 3$ -null pericyte-derived CXCL1, CCL2 and TIMP-1 on enhanced tumor cell survival and tumor growth, $\beta 3$ -null pericytes with CRISPR-Cas9 depletion of CXCL1, CCL2 or TIMP-1 ($\beta 3$ -null;CXCL1^{KO}, $\beta 3$ -null;CCL2^{KO} and $\beta 3$ -null;TIMP-1^{KO} respectively) were generated and target protein depletion confirmed by western blotting (**Figure 6 H**). Similar to the effect of deletion of Akt and HGFR in $\beta 3$ -null pericytes, exposure of B16F0 cells to conditioned medium from $\beta 3$ -null;CXCL1^{KO}, $\beta 3$ -

null;CCL2^{KO} and β 3-null;TIMP-1^{KO} pericytes reduced B16F0 cell survival significantly compared with enhanced survival induced by exposure to conditioned medium from β 3-null;Cas9 pericytes (**Figure 6 I**). This effect on enhancing tumor cell survival was corroborated *in vivo* where tumor growth was reduced when co-injecting B16F0 cells with either β 3-null;CXCL1^{KO}, β 3-null;CCL2^{KO} or β 3-null;TIMP-1^{KO} pericytes compared with co-injection of B16F0 cells with β 3-null;Cas9 pericytes (**Figure 6 J**). Together these data suggest that the depletion of these factors in β 3-null pericytes is sufficient to reduce the enhanced tumor growth observed and implicates them functionally, downstream of NF κ B activity, as pericyte-derived paracrine signals that regulate tumor growth.

Since the fold expression increase in β 3-null pericyte cytokine expression was highest for CCL2 (4-fold increase compared with WT pericytes, see figure 5D) and that I κ -B α SR transfection of β 3-null cells reduced CCL2 expression the most (4-fold decrease compared with mock transfected pericytes in figure 6E) we examined whether tumor cell CCR2, the receptor for CCL2, is involved in the enhanced tumor cell survival phenotype. B16F0 cells were exposed to conditioned media from WT and β 3-null pericytes and also treated with the CCR2i inhibitor or vehicle alone. Inhibition of CCR2 was sufficient to reduce the enhanced tumor cell survival observed after exposure to β 3-null pericyte conditioned medium suggesting that CCR2 is involved in tumor cell survival after exposure to β 3-null pericyte conditioned medium (**Supplementary figure 6 C**).

Using phosphoproteomic analysis of malignant cells, the molecular mechanism underlying the enhanced tumor cell survival and growth after exposure to β 3-null pericytes was examined. Kinase substrate enrichment analysis of phosphoproteomics data identified that the ROCK2 signalling pathway was the most significantly enriched pathway in tumor cells exposed to β 3-null pericyte conditioned medium compared with tumor cells exposed to WT pericyte conditioned medium (**Figure 7 A**). Phosphorylation levels of a number of proteins involved in tumor cell survival and progression supporting the notion that paracrine signals from β 3-null pericytes enhanced cell survival based signalling in tumor cells (**Supplementary figure 6 D**).

Non-muscle Myosin II has contractile properties and is regulated by phosphorylation of its light and heavy chains (Vicente-Manzanares et al., 2009). Importantly, a key phospho-substrate for many of the kinases arising from phosphoproteomic analysis was Myosin Light Chain 2 (MLC2, MYL12b and MYL9). Myosin II-driven contractility relies on multiple kinases. Amongst them, previously published work has shown that Rho-kinase (ROCK) inactivates the myosin light chain 2 (MLC2) phosphatase, which leads to increased phosphorylation of MLC2 (p-MLC2) and activity of Myosin II (Ito et al., 2004). MLC2 is also directly phosphorylated by ROCK (Vicente-Manzanares et al., 2009). Importantly, tumors arising from C57BL/6 mice injected with B16F0 melanoma cells plus β 3-null pericytes showed increased levels of p-MLC2 protein (a

direct substrate of ROCK) when compared with B16F0s co-injected with WT pericytes (**Figure 7 B**). These data indicate that tumors with $\beta 3$ -null pericytes grow with higher levels of actomyosin contractility, a feature associated with faster tumor growth *in vivo* (Georgouli et al., 2019). Given that previous reports demonstrated that MEK1 and MAPK cascade signalling pathways are downstream of CCL2/CCR2 stimulated signalling (Fang et al., 2012; Tang and Tsai, 2012), we examined whether loss of $\beta 3$ -null-pericyte-derived CCL2 was responsible for the enhancement of MEK1 and ROCK2 signalling pathways in B16F0. Western blot analysis showed reduced levels of p-MEK1/2, pERK1/2 and p-MLC2 in B16F0 cells exposed to conditioned medium from $\beta 3$ -null;CCL2^{KO} pericytes compared with B16F0 cells exposed to $\beta 3$ -null;Cas9 pericyte conditioned medium (**Figure 7 C**). These data suggest that CCL2 was involved in enhanced MEK1 and ROCK2 activity in tumor cells. Additionally, B16F0 tumors co-injected with $\beta 3$ -null;CCL2^{KO} pericytes showed a decrease in p-MLC2 levels, further linking a role for CCL2 in enhanced ROCK2-Myosin II activation *in vivo* (**Figure 7 D**).

To test the functional role of ROCK2 and MEK1 in enhancing tumor cell survival, tumor cells were treated with a MEK1 inhibitor (U0126) or ROCK inhibitor (GSK269962A) after exposure to $\beta 3$ -null pericytes. Reduced Myosin II or ERK1/2 activity were confirmed after treatment (**Figure 7 E**). B16F0 cells pre-treated with the U0126 MEK1-inhibitor or the GSK269962A ROCK-inhibitor displayed reduced tumor cell survival after exposure to $\beta 3$ -null pericyte conditioned medium compared to WT-pericyte conditioned medium (**Figure 7 F**). shRNA knockdown of ROCK2 in B16F0 cells resulted in reduced Myosin II activity (**Supplementary figure 6 E**). Although B16F0;ROCK2^{KO} cells did not have compromised growth *in vitro* (**Supplementary figure 6 F**), depletion of ROCK2 in B16F0 cells was sufficient to reduce tumor growth in *pdgfr β cre+; $\beta 3^{fl/fl}$* mice back to that observed in B16F0;ROCK2^{WT} or B16F0;ROCK2^{KO} tumor growth in *pdgfr β cre-; $\beta 3^{fl/fl}$* mice (**Figure 7 G**). These data confirm that the enhanced B16F0 tumor growth observed in absence of pericyte $\beta 3$ -integrin is dependent on B16F0 ROCK2 activity. The relationship between MEK1 and ROCK2 activation has been reported previously (Arozarena et al., 2011; Vial et al., 2003), Orgaz et al, 2019 *Cancer Cell* In Press. Together these results demonstrate a functional role for tumor cell MEK1 and ROCK2-Myosin II signalling in the enhanced tumor cell survival and tumor cell growth after exposure to $\beta 3$ -null pericytes.

DISCUSSION

Our data establish that mural cells, by losing $\beta 3$ -integrin expression, thus enhancing signalling via the FAK-HGFR-Akt-NF- κ B pathway and increasing CCL2 mediated paracrine signals can increase tumor burden via tumor cell enrichment of MEK1 and ROCK2 signalling pathways in the absence of affecting tumor blood vessel numbers or functionality. These results are not expected and call for consideration of the role of tumor pericytes in the direct control of tumor growth and progression.

Previous work has established that pericytes play critical roles in blood brain barrier function, vascular development, the control of vessel contraction, blood flow and haemostasis (Armulik et al., 2011; Raza et al., 2010). Based on these accepted functions as essential blood vessel supporting cells, elimination of pericytes was considered to be a logical anti-angiogenic strategy to control cancer. Indeed, antagonists of platelet derived growth factor signalling were shown to eliminate tumor pericytes resulting in vascular disruption and effective tumor regression (Heldin, 2013). However, similar strategies also result in enhancing vessel leakage and hypoxia thereby elevating metastasis (Cooke et al., 2012; Keskin et al., 2015; Xian et al., 2006). Thus targeting pericytes and inducing vascular disruption is unlikely to be a long term effective method of cancer control. Indeed, more recent reports have suggested that cancer progression can be associated with either increased or reduced pericyte association with tumor blood vessels (Cooke et al., 2012; Furuhashi et al., 2004; O'Keeffe et al., 2008; Sennino et al., 2007; Sinha et al., 2016; Xing et al., 2015; Yonenaga et al., 2005). Together these apparently conflicting data suggest that vascular disruption, or even enhanced blood vessel leakage via the loss of pericytes, may not be an effective method to control cancer. Indeed, they suggest that pericytes might control tumor growth through other mechanisms that have not been investigated carefully until now.

Loss of pericyte adhesion properties are likely to affect their association and recruitment to endothelial cells of the blood vessel wall. Integrins are a family of cell adhesion molecules that control cell-extracellular matrix interactions. Pericytes are known to express a variety of integrins including both $\beta 1$ - and $\beta 3$ -integrin heterodimers and reduced pericyte $\beta 1$ -integrin activity and, $\alpha 4$ - or $\alpha 6$ -integrin levels have all been shown to affect blood vessel maturation processes (Garmony-Susini et al., 2005; Reynolds et al., 2017; You et al., 2014), however the role of $\beta 3$ -integrin in pericyte function was unknown.

Our data demonstrate that loss of pericyte- $\beta 3$ -integrin is sufficient to enhance tumor growth in the absence of changes in blood vessel density, pericyte recruitment vessel perfusion or tumor hypoxia. Previous work has demonstrated that global deletion of $\beta 3$ -integrin is sufficient to enhance tumor angiogenesis and tumor growth (Reynolds et al., 2002) and that deletion of endothelial cell $\beta 3$ -integrin only transiently inhibits tumor angiogenesis in established tumors (Steri et al., 2014). This enhanced angiogenesis was proposed to be due to elevated VEGF-

induced responses of $\beta 3$ -null endothelial cells because of the up-regulated VEGF-receptor 2 expression on these cells (Reynolds et al., 2004; Reynolds et al., 2002). Our current study suggests that the mechanisms that control tumor growth in the pericyte-specific- $\beta 3$ -integrin knockout mice are distinct from those in global or endothelial cell-specific knockouts since the enhanced tumor growth is not associated with elevated angiogenesis. Thus explaining how pericyte- $\beta 3$ -integrin controls tumor growth was explored.

Our data point towards a possible new role for mural cells in directly affecting tumor growth and that this is controlled by $\beta 3$ -integrin expression. This conclusion is supported by clinical evidence where we show that a high percentage of blood vessels that are mural- $\beta 3$ -integrin negative is significantly associated with increased tumor size and progression in four different human cancers, including cutaneous melanoma, mesothelioma, lymphoma and breast cancer, without affecting blood vessel density.

Previous studies from other laboratories, and our own, have demonstrated that vascular endothelial cells can control tumor progression and chemosensitivity without affecting tumor angiogenesis *per se* via paracrine signals, namely angiocrine signals, that include cytokines and chemokines (Acharyya et al., 2012; Gilbert and Hemann, 2010; Tavora et al., 2014). These findings have indicated that vascular cells can regulate tumor growth in a way beyond their roles simply in vessel development and maintenance. Our mouse models show that loss of pericyte- $\beta 3$ -integrin is sufficient to enhance tumor growth via paracrine signals independent of tumor blood vessel function or numbers. Indeed, loss or inhibition of pericyte- $\beta 3$ -integrin expression significantly enhanced the FAK-p-HGFR-p-Akt-p-p65-CCL2 pathway. Interestingly, FAK and Akt are known regulators of cytokine production and angiocrine signalling (LaBarbera et al., 2015; Perkins, 2012; Tavora et al., 2014). Importantly, the clinical relevance of these findings was supported by elevated mural cell Akt- and p65-phosphorylation in human melanoma, lymphoma and breast cancer patients that had a high proportion of mural- $\beta 3$ -integrin negative blood vessels. Furthermore, the expression of CXCL1, CCL2 and TIMP-1 were all confirmed to be regulated by NF- κ B activation, suggesting that these paracrine factors, controlled by NF- κ B, could be at least part of the explanation of how $\beta 3$ -null pericytes regulate tumor growth. Within tumor cells, inactivation of ROCK2 in B16F0 tumor cells rescued the paracrine effects of $\beta 3$ -null pericytes on tumor growth both *in vitro* and *in vivo* suggesting that inhibition of ROCK2 in cancers with low pericyte- $\beta 3$ -integrin expression could be a novel way to control cancer growth and progression. Given that this increase in tumor cell survival was evident even in the absence of other cell types, suggests that the mural cell-derived factors can control tumor cell survival independent of blood flow or other cell types.

Overall, our study indicates that mural cells are not simply vessel supporting cells but that, via $\beta 3$ -integrin, can regulate tumor growth via mural-derived paracrine signals. Our data provide

proof-of-principle for a new role of mural cells, and shed light on a new mechanism of tumor growth control.

ACKNOWLEDGEMENTS

The authors would like to thank Barts Cancer Institute members Julie Holdsworth and Bruce Williams for their technical assistance; Jane Sosabowski for their technical advice on microCT imaging; Professor Ralf Adams (Max Planck Institute for Molecular Biomedicine, Münster, Germany) provided the *pdgfr β cre*⁺ mice. Professor Katherine Weilbaeher generated and provided us with the *β 3^{fl/m}* mice. Dr. St  phanie Kermorgant for her technical advice on HGFR inhibitor experiments. Dr. Ilaria Malanchi and Anna Pedrix for providing shRNA reagents. This work was supported by grants from: the Natural Science Foundation of China (81920108028, 81872142); Guangzhou Science and Technology Program (201904020008); the Key Training Program for Young Scholars of Sun Yat-Sen University (18ykzd07); Guangdong Science and Technology Department (2017B030314026); CRUK C8218/A18673; Worldwide Cancer Research (16-0390); Worldwide Cancer Research (19-0108); British Heart Foundation (FS/14/66/31293). N.C.H. is supported by a Wellcome Trust Senior Research Fellowship in Clinical Science (ref. 103749). H.K and P.M. are funded by Programme Grants from Breast Cancer Now as part of Programme Funding to the Breast Cancer Now Toby Robins Research Centre. P.M. acknowledges NIHR funding to the Royal Marsden Hospital Biomedical Research Centre (BRC).

AUTHOR CONTRIBUTIONS

P.-P. W. and J.M-F carried out the majority of the experiments, designed, conceived the project and wrote the paper; M.H and P.R.C performed the mass spectrometry analysis. H.K. and P.M. established the CRISPR-KO pericytes. Y-M.M and M.M did the triple-immunostaining of breast cancer tissues. B.D.L helped with the cell signaling studies. S.R. initiated the *pdgfr β cre*⁺; *β 3^{fl/m}* colonies; I.R. established the B16F0 ROCK2^{KO} cell lines. O.M. performed and analysed the p-MLC2 staining in tumors. N.B. carried out the collagen staining and quantitation; M.S.D. did the pimonidazole staining; L.R. helped with the TdTom and mTmG tissue analysis. G.E. did the histology; K.M and N.H provided the *TdTom*;*pdgfr β cre*⁻ and *TdTom*;*pdgfr β cre*⁺ unchallenged skin tissue. A.C. and J.G.G. provided human lymphoma tissue sections; S.D, S.M. and J.L.J. provided human breast cancer tissue; The authors wish to acknowledge the role of the Breast Cancer Now Tissue Bank in collecting and making available the samples used in the generation of this publication. P.W.S and C.H. provided the human mesothelioma and melanoma sections respectively; PZ, TJS, YW, JJC and RS developed and characterized the chemokine receptor inhibitor and JJC and RS coordinated collaboration between K.H.-D. and Chemocentryx; V.S.-M. helped interpret the ROCK2 data and helped write the paper; K.H.-D. designed and conceived the study, supervised the project and wrote the paper.

STAR * METHODS

Detailed methods are provided in the online version of this paper and include the following:

KEY RESOURCES TABLE

See separate document

CONTACT AND REAGENT RESOURCE SHARING

Further information requests and reagents should be directed to and will be fulfilled by the Lead Contact, Kairbaan Hodivala-Dilke (k.hodivala-dilke@qmul.ac.uk)

HUMAN SAMPLE COLLECTION AND PATIENT INFORMATION

Human ER+ breast cancer samples were obtained from the Barts Cancer Institute Breast Cancer Now tissue Bank and were covered by Research Tissue Bank Ethics Approval (Ethnic code 15/EE/0192). Human melanoma, mesothelioma and diffuse large B-cell lymphoma (Ethnic code 05/Q0605/140) samples were obtained with signed informed consent from patients and ethical committee approval.

Animal Models

pdgfr β cre mice were obtained from Professor Ralf Adams (Max Planck Institute for Molecular Biomedicine, Münster, Germany). *β 3^{fl/fl}* mice were generated by Professor Katherine Weilbaecher (Morgan et al., 2010). *pdgfr β cre-; β 3^{fl/fl}* and *pdgfr β cre+; β 3^{fl/fl}* mice were maintained on a pure C57 background for experiments. *β 3^{fl/fl}* mice were bred with *RIPtag-2* mice provided by Professor Douglas Hanahan, generating both male and female mice were used. mTmG mice were obtained from Cancer Research UK. mTmG mice were crossed with *pdgfr β cre+* mice to generate *pdgfr β cre-;mTmG* and *pdgfr β cre+;mTmG* mice for Cre-specificity analysis. Unchallenged adult skin from *TdTom;pdgfr β cre+* and *TdTom;pdgfr β cre-* control mice, fixed in 4% formalin, sucrose infiltrated, and snap frozen in OCT were used to assess *pdgfr β* -driven cre activity in skin mural cells.

METHOD DETAILS

Human tissue sections

Formalin fixed paraffin embedded tissue samples from human melanoma, diffuse large B-cell lymphoma, breast cancer and mesothelioma were sectioned, dewaxed, and antigen retrieval carried out in boiling 10 mM citrate buffer pH 6.0, 4 μ m sections were washed three times in PBS, blocked in 1% normal goat serum (NSG) 0.1% TritonX-100 (TX-100) for 1 h. Sections were double or triple immunostained for mouse monoclonal anti-alpha-smooth muscle actin Cy3-conjugated (Sigma-Aldrich-#C6198) and for either rabbit monoclonal anti-CD31 (Abcam-#ab76533), rabbit monoclonal anti-phospho-Akt (ser 473) (Cell Signaling Technology-#3787), rabbit monoclonal anti-NF- κ B p65 (Cell Signaling Technology-#8242), rabbit monoclonal anti-

β 3-integrin (Abcam-#ab75872) or rabbit polyclonal anti-CD61 (ThermoFisher Scientific-#PA5-32890). Sections were then washed three times with PBS, incubated with Alexa® 488-/546-conjugated anti-rabbit diluted 1:200 in 1% NGS 0.1% TX-100, washed three times and mounted with Prolong Gold Anti-Fade Mountant with DAPI (ThermoFisher Scientific-#P36931). For triple immunostaining, the tissue sections were further processed by using Tyramide SuperBoost™ Kit (Invitrogen-#B4093) combined with IHC (TSA-IHC). Different primary antibodies were sequentially applied, followed by horseradish peroxidase-conjugated secondary antibody incubation and tyramide signal amplification. The slides were microwave heat-treated after each TSA operation.

For data analysis, the percentage of β 3-integrin or p-Akt or p65 and α -SMA-double-positive blood vessels was calculated as the number of β 3-integrin or p-Akt or p65 and α -SMA-double-positive blood vessels over the total number of α -SMA-positive blood vessels. Patient data are expressed as those with either less, or more, than 50% of blood vessels that are mural β 3-integrin negative.

PCR genotyping

The primers for the Cre PCR: forward primer: 5'-GCTGTAGACGTAGTAAGTATCG-3'; reverse primer: 5'-GCTGGAGTTTCAATACCGGAG-3'. The reaction generates a fragment of approximately 669 bp. The primers for the *β 3-floxed* PCR: forward primer: 5'-TTGTTGGAGGTGAGCGAGTC-3' and reverse primer: 5'-GCCCAGCGGATCTCCATCT-3'. The PCR reaction generates a 272 bp fragment for the *β 3-floxed* allele and a 182 bp fragment for the *wild-type* allele. All the primers were purchased from ThermoFisher Scientific. For PCR reactions, the 25 μ l reactions contain 21 μ l MegaMix-Blue (MicroZone, Client life science), 100 ng DNA, 1 μ l of 10 nM forward and reverse primers respectively. For Cre PCR, the PCR program was run as a simplified hot start PCR with initial denaturation at 95 °C for 5 min, 35 cycles of 30 s at 95 °C, 1.5 min at 60 °C and 1 min at 72 °C, followed by a final extension for 5 min at 72 °C. For *β 3-floxed* PCR, the PCR program was run with initial denaturation at 95 °C for 2 min, 35 cycles of 30 s at 95 °C, 30 s at 56 °C and 30 s at 70 °C, followed by a final extension for 8 min at 72 °C. The thermocycler used were GeneAmp PCR systems 9700 (Applied Biosystems). 20 μ l of the PCR products were separated by electrophoresis on a 1.8% agarose gel, stained with ethidium bromide (0.25 μ g/ml) and viewed by a gel image system (BioRad, Germany).

Cell lines

Lewis lung carcinoma (LLC), B16F0 (melanoma, derived from C57BL/6), B16F10 (melanoma, derived from C57BL/6), E0771 (breast cancer, derived from C57BL/6) (all from ATCC). LLC, B16F0 and B16F10 were cultured in DMEM supplemented with 10% fetal bovine serum (Gibco 10500 (batch 07Q8041K) Pencillin and Streptomycin. E0771 cells were grown in RPMI

supplemented with 10% fetal bovine serum (Gibco 10500 (batch 07Q8041K) Pencillin and Streptomycin. Cell lines were maintained in a 5% CO₂ incubator at 37°C.

Mouse tumor models

All in vivo experiments have been performed according to Arrive Guidelines. 12-14 week old *pdgfr β cre-;* β 3^{fl/fl} and *pdgfr β cre+;* β 3^{fl/fl} mice were given a subcutaneous injection of either 1 x 10⁵ Lewis lung carcinoma (LLC) or B16F0 (melanoma, derived from C57BL/6) into the flank for subcutaneous tumor growth. Tumor growth was measured by using callipers every two days. Tumor volume (V) was calculated: V= (Length x width²) x 0.52. After 20-26 days, animals were culled, tumors excised and either fixed in 4% formaldehyde in PBS overnight, or snap frozen in liquid nitrogen for subsequent immunohistochemical analysis. For experimental metastasis assays, 5 x 10⁵ LLC or B16F10 melanoma cells were injected via the tail vein of *pdgfr β cre-;* β 3^{fl/fl} and *pdgfr β cre+;* β 3^{fl/fl} mice. Lung tumor burden was measured by a Nano SPECT/CT® *In vivo* preclinical imager (Bioscan) 3-4 times over 16 days according to the manufacturer's instruction (Wong et al., 2015). For breast cancer orthotopic model, 1 x 10⁵ E0771 cells were orthotopically injected into mammary fat pad of *pdgfr β cre-;* β 3^{fl/fl} and *pdgfr β cre+;* β 3^{fl/fl} mice. *RIPTag-2;**pdgfr β cre-;* β 3^{fl/fl}; and *RIPTag-2;**pdgfr β cre+;* β 3^{fl/fl}; were culled at 13 weeks of age. At necropsy, pancreas with peri-pancreatic lymph nodes, were fixed in 4% formaldehyde in PBS or snap frozen for subsequent immunohistochemical analysis.

For co-injection tumor growth assays, wild type C57BL/6 mice (Charles River) were intravenously co-injected with 1 x 10⁵ B16F10 cells and either 4 x 10⁵ WT or β 3-null pericytes, or with 1 x 10⁵ B16F10 cells and either 8 x 10⁵ WT or β 3-null pericytes. Three weeks post injection, the mice were sacrificed and the number of metastases in their lungs was counted. For breast cancer orthotopic model, 1 x 10⁵ E0771 cells were co-injected with either 4 x 10⁵ WT or β 3-null pericytes into the mammary fat pad of wild type C57BL/6 mice. To perform metastasis analysis, the tumor bearing mice were harvested when their primary tumor sizes reached 600 mm³, and their lungs were fixed for further metastasis analysis.

For *in vivo* rescue experiment, β 3-null pericytes were transfected using the Nucleofector® electroporation system (Lonza) with either the empty vector (mock control) or I κ -B α SR (kindly provided by Professor Neil Perkins) for 48 h. Wild type C57BL/6 mice were intravenously co-injected with 1 x 10⁵ B16F10 cells and either 4 x 10⁵ mock transfected- or I κ -B α SR transfected- β 3-null pericytes. Three weeks post injection, mice were sacrificed and the number of metastases in their lungs was quantified by counting the average of the number of metastases across entire lung H&E stained section area from three different levels of the lungs, with 10 μ m separation between each level. H&E stained sections from E0771 metastases and RIPTag-2 metastases were used to assess metastatic burden.

***In vivo* cell tracking**

B16F10 melanoma, WT or $\beta 3$ -null pericytes, previously labelled with CellTracker™ Red CMTPX Dye (Molecular probes, Invitrogen, Life Science), were resuspended at 0.5×10^6 cells per 100 μ l of PBS and injected via the tail vein into mice. At 2 or 48 h post inoculation, mice were sacrificed and lungs were fixed and processed as previously described (Batista et al., 2014). Lungs were dissected, photographed using a Leica M16F fluorescence stereomicroscope, snap-frozen in OCT (Killik, Bio-Optica, IT) and 4 μ m cryosections were prepared for analysis. Total number of CMTPX positive tumor cells or pericytes were quantified by counting the average of the number of CMTPX positive cells across entire lung section area from three different levels of the lungs (with 10 μ m separation between each level), using a Zeiss Axioplan microscope (Zeiss).

Immunofluorescence

Mouse tissues were fixed in formalin for 24 hr and transferred to 70% ethanol. The tissues were then paraffin embedded, sectioned, dewaxed, and unmasked in boiling 10 mM citrate buffer pH 6.0. 5 μ m sections were washed three times in PBS, blocked in 1% normal goat serum (NSG) 0.1% TritonX-100 (TX-100) for 1 hr. Sections were double immunostained for mouse monoclonal anti-alpha-smooth muscle actin Cy3-conjugated (Sigma-Aldrich-C6198) and for either rat monoclonal anti-endomucin (Santa Cruz Biotechnology-#sc-65495) or rabbit monoclonal anti- $\beta 3$ -integrin (Abcam-#ab75872). Sections were washed three times with PBS, incubated with Alexa® 488-/546-conjugated anti-rabbit or Alexa® 488-conjugated anti-rat secondary antibody (Invitrogen) diluted 1:200 in 1% NGS 0.1% TX-100, washed three times and mounted with Prolong Gold anti-Fade Mountant with DAPI. The percentage of α -SMA-positive blood vessels with $\beta 3$ -integrin expression was calculated as described previously. For collagen IV (rabbit polyclonal anti-collagen IV (Abcam-#ab6586))/endomucin (rat monoclonal anti-endomucin (Santa Cruz Biotechnology-#sc-65495)) and $\beta 3$ -integrin (rabbit polyclonal anti-CD61 (ThermoFisher Scientific-#PA5-32890))/PDGFR β (rabbit monoclonal anti-PDGFR β (Cell Signaling Technology-#3169) double immunostaining experiments, mouse tumors were snap-frozen, sectioned and fixed in ice-cold acetone for 10 min. 4 μ m sections were blocked for 45 min with 1.0% bovine serum albumin (BSA) and 0.1% Tween 20 in PBS. Primary antibodies were incubated overnight at 4°C followed by incubation with Alexa 546-conjugated secondary antibody for 1 h at RT (Invitrogen) diluted 1:200 in 1.0% bovine serum albumin (BSA) and 0.1% Tween 20 in PBS, washed three times and mounted with Prolong Gold anti-Fade Mountant with DAPI (ThermoFisher Scientific). *TdTom;pdgfr β cre-* and *TdTom;pdgfr β cre+* mouse unchallenged skin tissues were obtained from Neil Henderson lab (University of Edinburgh).

In vitro, cells were fixed with 4% formaldehyde in PBS for 10 min at RT. Rabbit monoclonal anti-phospho-NF- κ B p65 (Ser 536) (Cell Signaling Technology-#3033) antibody was incubated overnight at 4°C and washed three times with PBS followed by incubation with Alexa® 546-

conjugated secondary antibody (Invitrogen) for 1 h at RT diluted 1:200 in 1.0% bovine serum albumin (BSA) and 0.1% Tween 20 in PBS, washed three times and mounted with Prolong Gold anti-Fade Mountant with DAPI (ThermoFisher Scientific).

Blood vessel density and pericyte coverage

The number of endomucin-positive blood vessels present across the entire area of each mid-line tumor section from size and age-matched tumors or unchallenged skins was counted and divided by the area of the section to determine tumor blood vessel density.

For pericyte coverage, the percentage of α -SMA-positive, endomucin-positive blood vessels were counted.

Vascular perfusion

Vascular perfusion was visualized by injecting mice via the tail vein with PE-conjugated 20 μ g of rat monoclonal anti-PE-PECAM (BioLegend-#102408) 10 min prior to culling. Tumors were snap frozen, sectioned and stained for endomucin. The ratio (%) of double-positive blood vessels over endomucin-positive vessels provided an indication of blood vessel perfusion.

Hypoxia quantification (Pimonidazole) and vessel leakage (Hoechst diffusion)

Hypoxia and extravascular diffusion (vessel leakage) were tested by injecting mice with pimonidazole (Hypoxyprobe™-1 Kit) intraperitoneally 1 h prior to culling, and followed by intravenous injection of Hoechst dye (0.4 mg, Sigma-Aldrich) 1 min prior to culling and anti-PE-PECAM as above. Tumors were snap frozen, sectioned and fixed in ice-cold acetone for 10 min. 100 μ m thick frozen tumor sections were incubated overnight at 4 °C with a FITC-conjugated mouse monoclonal anti-pimonidazole (Hydroxyprobe HPI Burlington-#MA01803), and then washed and mounted. Sections were analyzed using confocal microscopy (LSM710, Carl Zeiss). Confocal stacks of 100 μ m were taken at 0.5 μ m intervals (20x) on multiple fields using 488 nm laser to excite anti-pimonidazole, 543 nm laser to excite anti-PE-PECAM, and 740 nm Mai-Tai femtosecond pulsing laser to excite Hoechst. For Hoechst diffusion quantification, the mean areas for PE-PECAM and Hoechst staining for each 100 μ m stack was calculated using ImageJ software. The Hoechst dye diffusion leakage area was calculated relative to PE-PECAM stained vessel area. For hypoxia quantification, the hypoxia index was calculated as the area of pimonidazole staining intensity across the area of tumor section.

Blood vessel collagen IV assessment

The percentage of endomucin-positive vessels with collagen IV expression was calculated as the number of collagen IV and endomucin-double positive blood vessels over the total number of endomucin-positive blood vessels.

Phospho-MLC2 staining and digital analysis

Tumors were formalin-fixed and paraffin-embedded using standard protocols. 4 μ m thick sections were incubated at 60 C° for 20 min and then subjected to antigen retrieval using citric acid based antigen unmasking solution (1:100; Vector Laboratories-#H-3300) at 110 C° for 6 min in a Decloaking Chamber™ NxGen (Biocare Medical). Samples were blocked with Dual Endogenous Enzyme-Blocking Reagent (Dako-#S2003) for 10 min and then were incubated with rabbit polyclonal anti-phospho-MLC2 (1:50; Cell Signaling Technology-#3671) for 40 min at RT, washed and then incubated with biotinylated goat anti-rabbit secondary antibody (1:200; Vector Laboratories-#BA-1000) for 30 min at RT. Signal was then amplified using VECTASTAIN ABC HRP Elite kit (Vector Laboratories-#PK-6100;) for 20 min at RT and the reaction was developed using Vector® VIP Peroxidase (HRP) Substrate Kit (Vector Laboratories-#SK-4600) for 10 min at RT. Staining was counterstained with Hematoxylin.

Sections from tumor xenograft experiments were imaged using NanoZoomer S210 slide scanner (Hamamatsu, Japan). Staining quantification was performed using QuPath v0.1.2 (Bankhead et al., 2017). The entire whole-section images (WSI) were analysed performing positive cell detection, and three different thresholds were applied according to the intensity scores (0, 1, 2 and 3). Next, the software was trained by creating random trees classification algorithm combined with the intensity information, in order to differentiate tumor from stroma, necrosis and immune cells. Values used in the analysis correspond to the quantification of p-MLC2 in the tumor margins.

Ultrasound analysis of blood flow, volume and perfusion

High-resolution ultrasound imaging of B16F0 tumors using the Vevo® 2100 system with a MS250 transducer was performed according to manufacturer instruction (Visualsonics). For blood flow, volume and perfusion measurement, contrast-enhanced ultrasound imaging was performed according to manufacturer instructions (Vevo® 2100 system). Briefly, B16F0 tumor bearing *pdgfr β cre-; β 3^{fl/fl}* and *pdgfr β cre+; β 3^{fl/fl}* mice were administered with 100 μ l of bolus Vevo Micromarker suspension (VisualSonics) via tail vein using tail vein Micromarker™ catheter. The ultrasound images were processed and analyzed by using VevoCQ™ contrast quantification software.

Primary pericyte, endothelial cell and fibroblast isolation and culture

Primary mouse endothelial cells, fibroblasts and pericytes were isolated from mouse brains and maintained as previously described (Reynolds et al., 2017). Briefly, *pdgfr β cre-; β 3^{fl/fl}* and *pdgfr β cre+; β 3^{fl/fl}* mouse brains were minced, collagenase type I digested (Gibco-#17100017), strained through a 70 μ m cell strainer (BD Falcon) and the resulting cell suspension plated on flasks coated with a mixture of 0.1% gelatin (Sigma-Aldrich-#G9136), 10 μ g/ml fibronectin (Merck-Millipore-#FC010) and 30 μ g/ml rat tail collagen (Sigma-Aldrich). Endothelial cells were purified by a single negative (Rat monoclonal anti-mouse FC γ sort-RII/III; BD Biosciences-#553141) and two positive cell sorts (Rat monoclonal anti-mouse ICAM-2; BD Biosciences-

#553326), using DYNAL® sheep anti-rat IgG-conjugated magnetic beads (ThermoFisher Scientific-#11035). During preparation of primary endothelial cells, fibroblasts were isolated from the non-endothelial cell population that was generated during the first positive sorting. For all cell types, passaging occurred when cells reached 70% confluency. Cells were trypsinized, centrifuged, washed with PBS and re-plated on pre-coated flasks for endothelial cells and pericytes and non-coated flasks for fibroblasts. For culture conditions, fibroblasts were cultured in DMEM + 10% FCS to passage 4, endothelial cells in MLEC medium (Ham's F-12, DMEM (low glucose), 10% FCS, heparin and endothelial mitogen (Generon)) to passage 4-5. Pericytes were cultured in pericyte medium including supplied pericyte growth supplement, FBS and pen/strep (ScienCell-#0010) to passage 10.

Generation of CRISPR/Cas9-KO cells

SgRNAs were designed using the CRISPOR algorithm (<http://crispor.tefor.net>). sgRNA sequences targeting TIMP-1 (Gene ID: 21857), CXCL1 (Gene ID: 14825), CCL2 (Gene ID: 20296), Akt1 (Gene ID: 11651), and HGFR (Met) (Gene ID: 17295) (see table S1) were cloned into the pLenti-CRISPR-EGFP plasmid (Addgene-#75159) using BsmBI enzyme site. 5.0×10^5 cells were centrifuged at 300 g for 5 min and re-suspended in 100 μ l of R1 buffer (Invitrogen). CRISPR/Cas9-EGFP plasmid DNA (10 μ g) were added into the WT and β 3-null pericytes and loaded into a 100 μ l Neon electroporation tip (Invitrogen). Electroporation was performed using 1350 mV for 20 ms with 2 pulse program on the Neon Electroporator (ThermoFisher Scientific). After electroporation, cells were rescued in pre-warmed supplemented media in the 0.1% gelatin with collagen and fibronectin-coated plates. 48 h post transfection, cells were washed with phosphate-buffered saline (PBS) and harvested with 500 μ l of FACS buffer (1% BSA and 0.5 mM EDTA in PBS). A 488-nm diode laser was used for the detection of EGFP. In each sample, viable singlet cells were gated via forward-scatter (FSC) laser and side-scatter (SSC) and EGFP positive cells, regardless of expression levels, were sorted using a FACSaria™ III flow cytometer (BD Biosciences) at the Chelsea Flow Cytometry and Light Microscopy Facility.

Generation of B16F0;ROCK2^{KO} cell lines

ROCK2 knockdown in B16F0 melanoma cells was achieved using doxycycline inducible Tet-pLKO-neo lentiviral shRNA constructs (Addgene-#21916). shRNA sequences for ROCK2 (5'-GCATCTCTTGAAGAAACAAAT-3') and non-targeting shControl (5'-GCGCGATAGCGCTAATAATTT-3') were designed using The RNAi Consortium collection (MISSION® shRNA, Sigma-Aldrich) and plasmids were generated by GenScript USA Inc. For lentivirus generation, 2×10^6 HEK293T cells on p100 dishes were transfected with lentiviral vector (5 μ g) along with packaging vectors (pMDLg/pRRE (2.5 μ g), pRSV-Rev (2.5 μ g) and pMD2.G (2 μ g) (Addgene)) using Optimem-I and Lipofectamine 2000 (ThermoFisher Scientific). Supernatants with lentiviruses were collected 48 h after transfection, spun down and filtered (0.45 μ m). For lentiviral transduction, 2.5×10^5 melanoma cells were seeded in T25 flasks and infected with lentiviruses. Stable cells were selected with 500 μ g/ml G418 (Sigma-Aldrich).

Gene knock-down was induced by the presence of doxycycline in the culture media (2 µg/ml) for *in vitro* experiments.

FACS analysis

For characterization of primary mouse brain pericytes, pericytes were washed with PBS and trypsinized at 37°C. The cell suspensions were washed in medium containing serum and centrifuged at 1, 200 rpm for 3 min. Cells were washed with cold FACS buffer (1% BSA/PBS) and fixed with 4% formaldehyde for 10 min at room temperature. Cells were washed with FACS buffer and the cell suspensions were incubated with the following primary antibodies: Rabbit polyclonal anti-NG2, Alexa Flour®488 conjugated (Merck Millipore-#AB5320A4), Rat monoclonal PE-anti-CD31 (BioLegend-#102508), rat monoclonal PE-anti-CD11b (Mac1) (BioLegend-#101208), rat monoclonal APC-anti-PDGFR β (BioLegend-#136008), rat monoclonal APC-anti-PDGFR α (BioLegend-#135908), rat monoclonal PE/Cy7-anti-CD146 (BioLegend-#134714) for 30 min. Cells were then washed three times in sample buffer and re-suspended in a final volume of 400 µl. As a control, unstained cells were FACS sorted.

Proteome profiler phospho-receptor tyrosine kinase and tyrosine kinase arrays

WT and β 3-null pericytes were grown in normal pericyte media and the whole-cell lysates were extracted after 72 h incubation. Phospho-receptor tyrosine kinase and tyrosine kinase arrays (*Proteome-Profilers* ARY001B & ARY003B, R&D systems) were processed according to the manufacturer's instruction using 300 µg of lysates per membrane. Pixel analysis was used for quantification with Image J software.

Western blotting

Pericytes, endothelial cells or fibroblasts were harvested and lysed with NP40 lysis buffer (Invitrogen). Protein concentration was determined using the Bio-Rad Dc Protein Assay Kit (Bio-Rad Laboratories). 15-30 µg of protein from each sample was loaded onto 8-12% polyacrylamide gels. The protein was transferred to a nitrocellulose membrane and incubated for 1 h in 5% milk phosphate buffered saline with 0.1% Tween-20 (PBS-T), followed by an overnight incubation of primary antibody diluted 1:1000 in 2% milk PBS-T at 4°C. The blots were then washed three times with PBS-T and incubated with the relevant horseradish peroxidase (HRP)-conjugated antibody diluted 1:1000 in 2% milk in PBS-T, for 1h at RT. Chemiluminescence was detected by exposing the membrane to high performance Super XR film (Fujifilm, PYSER-SGI limited). Densitometry readings were calculated with ImageJ software. Hsc70 was used as loading control. The following antibodies were used: rat monoclonal anti-endomucin (Santa Cruz Biotechnology-sc-65495), rabbit monoclonal anti- β 3-integrin (Cell Signaling Technology-#4702), rabbit monoclonal anti- β 5-integrin (Cell Signaling-#3629), rabbit monoclonal anti- β 1-integrin (Cell Signaling Technology-#4706), rabbit monoclonal anti-PDGFR β (Cell Signaling Technology-#3169), rabbit polyclonal anti-NG2

(Merck Millipore-AB5320), rabbit monoclonal anti-NF- κ B p65 (Cell Signaling Technology-#8242), rabbit monoclonal anti-phospho-NF- κ B p65 (Ser 536) (Cell Signaling Technology-#3033), rabbit monoclonal anti-Akt (Cell Signaling Technology-#4691), rabbit monoclonal anti-phospho-Akt (Ser 473) (Cell Signaling Technology-#4060), mouse monoclonal anti-Hsc70 (Santa Cruz Biotechnology-#sc7298), goat polyclonal anti-MCP-1 (CCL2) (ThermoFisher Scientific-#PA5-46954), rat monoclonal anti-CXCL1 (ThermoFisher Scientific-#MA5-23811), mouse monoclonal anti-TIMP-1 (ThermoFisher Scientific-#MA5-13688), rabbit monoclonal anti-Myosin Light Chain 2 (Cell Signaling Technology-#3672), rabbit anti-phospho-FAK (Tyr397) (Cell Signaling Technology-#3283), mouse monoclonal anti-Met (HGFR) (Santa Cruz Biotechnology-#sc-8057), rabbit monoclonal anti-phospho-Met (HGFR) (Tyr1234/1235) (Cell Signaling Technology-#3077), mouse monoclonal anti-Akt1 (Cell Signaling Technology-#2967), rabbit polyclonal anti-phospho-MEK1/2 (Ser217/221) (Cell Signaling Technology-#9121), mouse monoclonal anti-Rock II (Biosciences-#610624).

Mass spectrometry-based phosphoproteomics

WT and β 3-null pericytes were seeded in 100 cm² Petri dishes at (1 x 10⁶ cells/ml) concentration. B16f0 cells were treated with CM from WT and β 3-null pericytes for 30 min and 24 h in 100 cm² Petri dishes (1 x 10⁶ cells/ml). Cells were washed twice with cold PBS supplemented with 1 mM Na₃VO₄ and 1 mM NaF and lysed in 500 μ l urea buffer (8 M urea in 20 mM in HEPES pH 8.0 supplemented with 1 mM Na₃VO₄, 1 mM NaF, 1 mM Na₄P₂O₇ and 1 mM sodium β -glycerophosphate). Cell lysates were homogenized by sonication for 15 cycles of 30 s on 35 s off (Diagenode Bioruptor® Plus, Liege, Belgium). Insoluble material was removed by centrifugation at 16,000 x g for 15 min at 4 °C and protein in the cell extracts was quantified by bicinchoninic acid (BCA) analysis (ThermoFisher Scientific-#23225).

For phosphoproteome analyses, we used published methods (Gruhler et al., 2005; Larsen et al., 2005; Montoya et al., 2011) . As they were eluted from the nano-LC system, peptides were infused into the online connected Q-Exactive Plus system operating with a 2.1 s duty cycle. Acquisition of full scan survey spectra (m/z 375-1,500) with a 70,000 FWHM resolution was followed by, data-dependent acquisition in which the 15 most intense ions were selected for HCD (higher energy collisional dissociation) and MS/MS scanning (200-2,000 m/z) with a resolution of 17,500 FWHM. A 30s dynamic exclusion period was enabled with an exclusion list with 10 ppm mass window. Overall duty cycle generated chromatographic peaks of approximately 30 s at the base, which allowed the construction of extracted ion chromatograms (XICs) with at least 10 data points. The mass spectrometry proteomics data have been deposited to the ProteomeXchange Consortium via the PRIDE (Vizcaino et al., 2016). Partner repository with the dataset identifier PXD014513 (project DOI 10.6019/ PXD014513)

Mascot Daemon 2.5.0 was used to automate peptide identification from MS data. Peak list files (MGFs) from RAW data were generated with Mascot Distiller v2.6.1.0 and loaded into the

Mascot search engine (v2.5) in order to match MS/MS data to peptides (Perkins et al., 1999). The searches were performed against the SwissProt Database (SwissProt_2018_09. fasta) with a FDR of ~1% and the following parameters: 2 trypsin missed cleavages, mass tolerance of ± 10 ppm for the MS scans and ± 25 mmu for the MS/MS scans, carbamidomethyl of Cys as a fixed modification, PyroGlu on N-terminal Gln and oxidation of Met and phosphorylation on Ser, Thr, and Tyr as variable modifications. The in-house developed Pescal software was used for label-free peptide quantification (Cutillas, 2017; Wilkes et al., 2017), XICs for all the peptides identified across all samples were constructed with ± 7 ppm and ± 2 min mass and retention time windows, respectively. Peak areas from all XICs were calculated. Undetectable peptides were given an intensity value of 0. Values of 2 technical replicates per sample were averaged and intensity values for each peptide were normalized to total sample intensity. Unpaired, two-tail Student's *t* test was used to assess significance in phosphoproteomics data.

***In vitro* inhibitor experiments**

For $\alpha v\beta 3$ -integrin inhibitor experiments, $\beta 3$ -null pericytes were treated with either placebo or 20 μ M Cilengitide (purchased from Bachem) for 24 h. For HGFR inhibitor experiments, $\beta 3$ -null pericytes were treated with either DMSO or 1 μ M HGFR inhibitor (PHA-665752, provided by Dr. St phanie Kermorgant) for 10, 30 and 60 min respectively. For Akt inhibitor experiments, $\beta 3$ -null pericytes were treated with either DMSO or 10 μ M Akt inhibitor (LY294002, Sigma-Aldrich-#L9908) for 10, 30 and 60 minutes respectively. For FAK inhibitor experiments, $\beta 3$ -null pericytes were treated with either DMSO or 10 μ M FAK inhibitor (PF573228, TOCRIS-#3239) for 24 hours respectively.

For MEK or ROCK inhibitor experiments, B16F0 cells were treated with either the conditioned medium from WT or $\beta 3$ -null pericytes in the presence of either DMSO, MEK inhibitor (U0126, TOCRIS-#1144) or ROCK inhibitor (GSK269962A, TOCRIS-#4009) for 3 days in MTS experiments and 3 days for *in vivo* experiments or 1 day for western blot analysis.

***In vitro* treatment of B16F0 cells with CCR2i**

CCR2i was discovered through structure-activity relationship modification of screening hits and synthesized by the Medicinal Chemistry Department at ChemoCentryx (Mountain View, CA) according to procedures described (Patent Application Numbers: WO 2014089495 and WO 2016187393). B16F0 cells were treated with conditioned medium from $\beta 3$ -null pericytes in combination or not with CCR2i for 48 h for MTS assays.

Cytokine arrays

WT and $\beta 3$ -null pericytes or transfected WT and $\beta 3$ -null pericytes were grown in normal pericyte media. After 72 h of transfection, the whole-cell lysates were extracted. Mouse cytokine arrays (Proteome-Profiler ARY006, R&D systems) were processed according to the manufacturer's

instruction using 300 µg of lysates per membrane as previously described (Tavora et al., 2014). Pixel analysis was used for quantification with Image J software.

Conditioned media production from WT/ β 3-null pericytes, Cas9, Akt^{KO}, HGFR^{KO}, CXCL1^{KO}, CCL2^{KO}, TIMP-1^{KO} or mock/ κ -B α SR transfected pericytes

WT and β 3-null pericytes were cultured with pericyte medium for 72 h. This medium was then collected and applied to B16F0, B16F10, LLC cells for 3 days at 37°C and tumor cell survival was assessed using the MTS assay as described later. For mock/ κ -B α SR-transfected pericyte medium, the pericytes were transfected using the Nucleofector® electroporation system (Lonza) with either the empty vector or κ -B α SR. After 72 h incubation, this medium was collected and applied to B16F0, B16F10, LLC cells for 3 days.

***In vitro* cell viability assays**

LLC, B16F0 or B16F10 cell survival was assessed using the CellTiter 96® Aqueous One Solution Reagent (Promega-#G3582), according to the manufacturer's instructions. Plates were read at a wavelength of 490 nm, with absorbance measured relative to blank wells containing reagent only.

Transwell invasion assays

Invasion assays were performed using transwell polycarbonate membranes (Sigma Aldrich). A suspension of 5×10^4 B16F0 cells in 100 µl OptiMEM was seeded in the upper chamber of the transwell, being the 8 µm-pore membrane pre-coated with 50 µl of collagen (3 mg/ml in serum free DMEM). The lower chamber was filled with conditioned medium from WT or β 3-null pericytes during 48 h. At the endpoint membranes were fixed with PFA 4% and stained with DAPI. Number of cells per field were quantified using using a Zeiss Axioplan microscope (Zeiss).

B16F0;ROCK2^{KO} *in vivo* tumor growth assays with doxycycline

pdgfr β cre-; β 3^{fl/fl} and *pdgfr β cre+;* β 3^{fl/f} were injected with 1×10^5 B16F0;ROCK2^{KO} cells or and B16F0;ROCK2^{WT} cells. Induction of the transgene in the cell lines *in vivo* was performed by administering doxycycline 2 mg/l in drinking water with 5% sucrose. The administration of doxycycline took place once the tumors were palpable (7 days after injection).

Animal ethical regulations

All animal procedures were approved by our local animal ethics committee, Queen Mary University of London and were executed in accordance with United Kingdom Home Office regulations.

LEAD CONTACT AND MATERIALS AVAILABILITY

Further information and requests for resources and reagents should be directed to and will be fulfilled by the senior author Kairbaan Hodivala-Dilke (k.hodivala-dilke@qmul.ac.uk).

REFERENCES

- Acharyya, S., Oskarsson, T., Vanharanta, S., Malladi, S., Kim, J., Morris, P.G., Manova-Todorova, K., Leversha, M., Hogg, N., Seshan, V.E., *et al.* (2012). A CXCL1 paracrine network links cancer chemoresistance and metastasis. *Cell* 150, 165-178.
- Armulik, A., Genove, G., and Betsholtz, C. (2011). Pericytes: developmental, physiological, and pathological perspectives, problems, and promises. *Dev Cell* 21, 193-215.
- Arozarena, I., Sanchez-Laorden, B., Packer, L., Hidalgo-Carcedo, C., Hayward, R., Viros, A., Sahai, E., and Marais, R. (2011). Oncogenic BRAF induces melanoma cell invasion by downregulating the cGMP-specific phosphodiesterase PDE5A. *Cancer Cell* 19, 45-57.
- Batista, S., Maniati, E., Reynolds, L.E., Tavora, B., Lees, D.M., Fernandez, I., Elia, G., Casanovas, O., Lo Celso, C., Hagemann, T., *et al.* (2014). Haematopoietic focal adhesion kinase deficiency alters haematopoietic homeostasis to drive tumour metastasis. *Nat Commun* 5, 5054.
- Brantley-Sieders, D.M., Dunaway, C.M., Rao, M., Short, S., Hwang, Y., Gao, Y., Li, D., Jiang, A., Shyr, Y., Wu, J.Y., *et al.* (2011). Angiocrine factors modulate tumor proliferation and motility through EphA2 repression of Slit2 tumor suppressor function in endothelium. *Cancer research* 71, 976-987.
- Brooks, P.C., Clark, R.A., and Cheresh, D.A. (1994a). Requirement of vascular integrin alpha v beta 3 for angiogenesis. *Science* 264, 569-571.
- Brooks, P.C., Montgomery, A.M., Rosenfeld, M., Reisfeld, R.A., Hu, T., Klier, G., and Cheresh, D.A. (1994b). Integrin alpha v beta 3 antagonists promote tumor regression by inducing apoptosis of angiogenic blood vessels. *Cell* 79, 1157-1164.
- Brooks, P.C., Stromblad, S., Klemke, R., Visscher, D., Sarkar, F.H., and Cheresh, D.A. (1995). Antiintegrin alpha v beta 3 blocks human breast cancer growth and angiogenesis in human skin. *J Clin Invest* 96, 1815-1822.
- Cao, Z., Ding, B.S., Guo, P., Lee, S.B., Butler, J.M., Casey, S.C., Simons, M., Tam, W., Felsher, D.W., Shido, K., *et al.* (2014). Angiocrine factors deployed by tumor vascular niche induce B cell lymphoma invasiveness and chemoresistance. *Cancer cell* 25, 350-365.
- Cao, Z., Scandura, J.M., Inghirami, G.G., Shido, K., Ding, B.S., and Rafii, S. (2017). Molecular Checkpoint Decisions Made by Subverted Vascular Niche Transform Indolent Tumor Cells into Chemoresistant Cancer Stem Cells. *Cancer cell* 31, 110-126.

Caspani, E.M., Crossley, P.H., Redondo-Garcia, C., and Martinez, S. (2014). Glioblastoma: a pathogenic crosstalk between tumor cells and pericytes. *PLoS one* 9, e101402.

Cheng, J., Phong, B., Wilson, D.C., Hirsch, R., and Kane, L.P. (2011). Akt fine-tunes NF- κ B-dependent gene expression during T cell activation. *J Biol Chem* 286, 36076-36085.

Chung, A.S., Lee, J., and Ferrara, N. (2010). Targeting the tumour vasculature: insights from physiological angiogenesis. *Nature reviews Cancer* 10, 505-514.

Cooke, V.G., LeBleu, V.S., Keskin, D., Khan, Z., O'Connell, J.T., Teng, Y., Duncan, M.B., Xie, L., Maeda, G., Vong, S., *et al.* (2012). Pericyte depletion results in hypoxia-associated epithelial-to-mesenchymal transition and metastasis mediated by met signaling pathway. *Cancer Cell* 21, 66-81.

Cutillas, P.R. (2017). Targeted In-Depth Quantification of Signaling Using Label-Free Mass Spectrometry. *Methods Enzymol* 585, 245-268.

Dan, H.C., Cooper, M.J., Cogswell, P.C., Duncan, J.A., Ting, J.P., and Baldwin, A.S. (2008). Akt-dependent regulation of NF- κ B is controlled by mTOR and Raptor in association with IKK. *Genes Dev* 22, 1490-1500.

Fang, W.B., Jokar, I., Zou, A., Lambert, D., Dendukuri, P., and Cheng, N. (2012). CCL2/CCR2 chemokine signaling coordinates survival and motility of breast cancer cells through Smad3 protein- and p42/44 mitogen-activated protein kinase (MAPK)-dependent mechanisms. *J Biol Chem* 287, 36593-36608.

Foo, S.S., Turner, C.J., Adams, S., Compagni, A., Aubyn, D., Kogata, N., Lindblom, P., Shani, M., Zicha, D., and Adams, R.H. (2006). Ephrin-B2 controls cell motility and adhesion during blood-vessel-wall assembly. *Cell* 124, 161-173.

Furuhashi, M., Sjoblom, T., Abramsson, A., Ellingsen, J., Micke, P., Li, H., Bergsten-Folestad, E., Eriksson, U., Heuchel, R., Betsholtz, C., *et al.* (2004). Platelet-derived growth factor production by B16 melanoma cells leads to increased pericyte abundance in tumors and an associated increase in tumor growth rate. *Cancer research* 64, 2725-2733.

Garmy-Susini, B., Jin, H., Zhu, Y., Sung, R.J., Hwang, R., and Varner, J. (2005). Integrin α 4 β 1-VCAM-1-mediated adhesion between endothelial and mural cells is required for blood vessel maturation. *J Clin Invest* 115, 1542-1551.

Georgouli, M., Herraiz, C., Crosas-Molist, E., Fanshawe, B., Maiques, O., Perdrix, A., Pandya, P., Rodriguez-Hernandez, I., Ilieva, K.M., Cantelli, G., *et al.* (2019). Regional Activation of Myosin II in Cancer Cells Drives Tumor Progression via a Secretory Cross-Talk with the Immune Microenvironment. *Cell* 176, 757-774 e723.

Ghajar, C.M., Peinado, H., Mori, H., Matei, I.R., Evason, K.J., Brazier, H., Almeida, D., Koller, A., Hajjar, K.A., Stainier, D.Y., *et al.* (2013). The perivascular niche regulates breast tumour dormancy. *Nat Cell Biol* 15, 807-817.

Ghiabi, P., Jiang, J., Pasquier, J., Maleki, M., Abu-Kaoud, N., Rafii, S., and Rafii, A. (2014). Endothelial cells provide a notch-dependent pro-tumoral niche for enhancing breast cancer survival, stemness and pro-metastatic properties. *PloS one* 9, e112424.

Gilbert, L.A., and Hemann, M.T. (2010). DNA damage-mediated induction of a chemoresistant niche. *Cell* 143, 355-366.

Gruhler, A., Olsen, J.V., Mohammed, S., Mortensen, P., Faergeman, N.J., Mann, M., and Jensen, O.N. (2005). Quantitative phosphoproteomics applied to the yeast pheromone signaling pathway. *Mol Cell Proteomics* 4, 310-327.

Guan, J.L. (2010). Integrin signaling through FAK in the regulation of mammary stem cells and breast cancer. *IUBMB Life* 62, 268-276.

Guerrouahen, B.S., Pasquier, J., Kaoud, N.A., Maleki, M., Beauchamp, M.C., Yasmeen, A., Ghiabi, P., Lis, R., Vidal, F., Saleh, A., *et al.* (2014). Akt-activated endothelium constitutes the niche for residual disease and resistance to bevacizumab in ovarian cancer. *Mol Cancer Ther* 13, 3123-3136.

Hanahan, D., and Weinberg, R.A. (2011). Hallmarks of cancer: the next generation. *Cell* 144, 646-674.

Heldin, C.H. (2013). Targeting the PDGF signaling pathway in tumor treatment. *Cell Commun Signal* 11, 97.

Ito, M., Nakano, T., Erdodi, F., and Hartshorne, D.J. (2004). Myosin phosphatase: structure, regulation and function. *Mol Cell Biochem* 259, 197-209.

Keskin, D., Kim, J., Cooke, V.G., Wu, C.C., Sugimoto, H., Gu, C., De Palma, M., Kalluri, R., and LeBleu, V.S. (2015). Targeting vascular pericytes in hypoxic tumors increases lung metastasis via angiopoietin-2. *Cell Rep* 10, 1066-1081.

LaBarbera, K.E., Hyldahl, R.D., O'Fallon, K.S., Clarkson, P.M., and Witkowski, S. (2015). Pericyte NF-kappaB activation enhances endothelial cell proliferation and proangiogenic cytokine secretion in vitro. *Physiol Rep* 3.

Larsen, M.R., Thingholm, T.E., Jensen, O.N., Roepstorff, P., and Jorgensen, T.J. (2005). Highly selective enrichment of phosphorylated peptides from peptide mixtures using titanium dioxide microcolumns. *Mol Cell Proteomics* 4, 873-886.

Lu, J., Ye, X., Fan, F., Xia, L., Bhattacharya, R., Bellister, S., Tozzi, F., Sceusi, E., Zhou, Y., Tachibana, I., *et al.* (2013). Endothelial cells promote the colorectal cancer stem cell phenotype through a soluble form of Jagged-1. *Cancer cell* 23, 171-185.

Mas-Moruno, C., Rechenmacher, F., and Kessler, H. (2010). Cilengitide: the first anti-angiogenic small molecule drug candidate design, synthesis and clinical evaluation. *Anticancer Agents Med Chem* 10, 753-768.

Mason, W.P. (2015). End of the road: confounding results of the CORE trial terminate the arduous journey of cilengitide for glioblastoma. *Neuro-oncology* 17, 634-635.

Montoya, A., Beltran, L., Casado, P., Rodriguez-Prados, J.C., and Cutillas, P.R. (2011). Characterization of a TiO₂ enrichment method for label-free quantitative phosphoproteomics. *Methods* 54, 370-378.

Morgan, E.A., Schneider, J.G., Baroni, T.E., Uluckan, O., Heller, E., Hurchla, M.A., Deng, H., Floyd, D., Berdy, A., Prior, J.L., *et al.* (2010). Dissection of platelet and myeloid cell defects by conditional targeting of the beta3-integrin subunit. *FASEB J* 24, 1117-1127.

Orgaz JL, Crosas-Molist E, Sadok A, Perdrix-Rosell A, Maiques O, Monger J, Rodriguez-Hernandez I, Mele S, Georgouli M, Bridgeman V, Karagiannis P, Pandya P, Cantelli G, Boehme L, Wallberg F, V Tape C, Karagiannis SN, Malanchi I, Sanz-Moreno V (2020) Myosin II reactivation and Cytoskeletal remodelling as a hallmark and a vulnerability in melanoma resistance. *Cancer Cell*, 37, 1-19 January 13. <https://doi.org/10.1016/j.ccell.2019.12.003>

O'Keeffe, M.B., Devlin, A.H., Burns, A.J., Gardiner, T.A., Logan, I.D., Hirst, D.G., and McKeown, S.R. (2008). Investigation of pericytes, hypoxia, and vascularity in bladder tumors: association with clinical outcomes. *Oncol Res* 17, 93-101.

Pedrosa, A.R., Trindade, A., Carvalho, C., Graca, J., Carvalho, S., Peleteiro, M.C., Adams, R.H., and Duarte, A. (2015). Endothelial Jagged1 promotes solid tumor growth through both pro-angiogenic and angiocrine functions. *Oncotarget* 6, 24404-24423.

Perkins, D.N., Pappin, D.J., Creasy, D.M., and Cottrell, J.S. (1999). Probability-based protein identification by searching sequence databases using mass spectrometry data. *Electrophoresis* 20, 3551-3567.

Perkins, N.D. (2012). The diverse and complex roles of NF-kappaB subunits in cancer. *Nature reviews Cancer* 12, 121-132.

Pietras, K., Rubin, K., Sjoblom, T., Buchdunger, E., Sjoquist, M., Heldin, C.H., and Ostman, A. (2002). Inhibition of PDGF receptor signaling in tumor stroma enhances antitumor effect of chemotherapy. *Cancer research* 62, 5476-5484.

Pikarsky, E., Porat, R.M., Stein, I., Abramovitch, R., Amit, S., Kasem, S., Gutkovich-Pyest, E., Urieli-Shoval, S., Galun, E., and Ben-Neriah, Y. (2004). NF-kappaB functions as a tumour promoter in inflammation-associated cancer. *Nature* 431, 461-466.

Poulos, M.G., Ramalingam, P., Gutkin, M.C., Kleppe, M., Ginsberg, M., Crowley, M.J., Elemento, O., Levine, R.L., Rafii, S., Kitajewski, J., *et al.* (2016). Endothelial-specific inhibition of NF-kappaB enhances functional haematopoiesis. *Nat Commun* 7, 13829.

Raza, A., Franklin, M.J., and Dudek, A.Z. (2010). Pericytes and vessel maturation during tumor angiogenesis and metastasis. *Am J Hematol* 85, 593-598.

Reynolds, A.R., Hart, I.R., Watson, A.R., Welte, J.C., Silva, R.G., Robinson, S.D., Da Violante, G., Gourlaouen, M., Salih, M., Jones, M.C., *et al.* (2009). Stimulation of tumor growth and angiogenesis by low concentrations of RGD-mimetic integrin inhibitors. *Nature medicine* 15, 392-400.

Reynolds, A.R., Reynolds, L.E., Nagel, T.E., Lively, J.C., Robinson, S.D., Hicklin, D.J., Bodary, S.C., and Hovav-Dilke, K.M. (2004). Elevated Flk1 (vascular endothelial growth factor receptor 2) signaling mediates enhanced angiogenesis in beta3-integrin-deficient mice. *Cancer research* 64, 8643-8650.

Reynolds, L.E., D'Amico, G., Lechertier, T., Papachristodoulou, A., Munoz-Felix, J.M., De Arcangelis, A., Baker, M., Serrels, B., and Hovav-Dilke, K.M. (2017). Dual role of pericyte alpha6beta1-integrin in tumour blood vessels. *J Cell Sci* 130, 1583-1595.

Reynolds, L.E., Wyder, L., Lively, J.C., Taverna, D., Robinson, S.D., Huang, X., Sheppard, D., Hynes, R.O., and Hovav-Dilke, K.M. (2002). Enhanced pathological angiogenesis in mice lacking beta3 integrin or beta3 and beta5 integrins. *Nat Med* 8, 27-34.

Robinson, S.D., and Hodivala-Dilke, K.M. (2011). The role of beta3-integrins in tumor angiogenesis: context is everything. *Current opinion in cell biology* 23, 630-637.

Sennino, B., Falcon, B.L., McCauley, D., Le, T., McCauley, T., Kurz, J.C., Haskell, A., Epstein, D.M., and McDonald, D.M. (2007). Sequential loss of tumor vessel pericytes and endothelial cells after inhibition of platelet-derived growth factor B by selective aptamer AX102. *Cancer research* 67, 7358-7367.

Sinha, D., Chong, L., George, J., Schluter, H., Monchgesang, S., Mills, S., Li, J., Parish, C., Bowtell, D., Kaur, P., *et al.* (2016). Pericytes Promote Malignant Ovarian Cancer Progression in Mice and Predict Poor Prognosis in Serous Ovarian Cancer Patients. *Clinical cancer research : an official journal of the American Association for Cancer Research* 22, 1813-1824.

Steri, V., Ellison, T.S., Gontarczyk, A.M., Weilbaecher, K., Schneider, J.G., Edwards, D., Fruttiger, M., Hodivala-Dilke, K.M., and Robinson, S.D. (2014). Acute depletion of endothelial beta3-integrin transiently inhibits tumor growth and angiogenesis in mice. *Circ Res* 114, 79-91.

Stratman, A.N., Malotte, K.M., Mahan, R.D., Davis, M.J., and Davis, G.E. (2009). Pericyte recruitment during vasculogenic tube assembly stimulates endothelial basement membrane matrix formation. *Blood* 114, 5091-5101.

Stupp, R., Hegi, M.E., Gorlia, T., Erridge, S.C., Perry, J., Hong, Y.K., Aldape, K.D., Lhermitte, B., Pietsch, T., Grujicic, D., *et al.* (2014). Cilengitide combined with standard treatment for patients with newly diagnosed glioblastoma with methylated MGMT promoter (CENTRIC EORTC 26071-22072 study): a multicentre, randomised, open-label, phase 3 trial. *The Lancet Oncology* 15, 1100-1108.

Stupp, R., and Rugg, C. (2007). Integrin inhibitors reaching the clinic. *Journal of clinical oncology : official journal of the American Society of Clinical Oncology* 25, 1637-1638.

Tang, C.H., and Tsai, C.C. (2012). CCL2 increases MMP-9 expression and cell motility in human chondrosarcoma cells via the Ras/Raf/MEK/ERK/NF-kappaB signaling pathway. *Biochemical pharmacology* 83, 335-344.

Tavora, B., Reynolds, L.E., Batista, S., Demircioglu, F., Fernandez, I., Lechertier, T., Lees, D.M., Wong, P.P., Alexopoulou, A., Elia, G., *et al.* (2014). Endothelial-cell FAK targeting sensitizes tumours to DNA-damaging therapy. *Nature* 514, 112-116.

Tucci, M., Stucci, S., and Silvestris, F. (2014). Does cilengitide deserve another chance? *The Lancet Oncology* 15, e584-585.

Usatyuk, P.V., Fu, P., Mohan, V., Epshtein, Y., Jacobson, J.R., Gomez-Cambronero, J., Wary, K.K., Bindokas, V., Dudek, S.M., Salgia, R., *et al.* (2014). Role of c-Met/phosphatidylinositol 3-kinase (PI3k)/Akt signaling in hepatocyte growth factor (HGF)-mediated lamellipodia formation, reactive oxygen species (ROS) generation, and motility of lung endothelial cells. *J Biol Chem* 289, 13476-13491.

Vial, E., Sahai, E., and Marshall, C.J. (2003). ERK-MAPK signaling coordinately regulates activity of Rac1 and RhoA for tumor cell motility. *Cancer Cell* 4, 67-79.

Vicente-Manzanares, M., Ma, X., Adelstein, R.S., and Horwitz, A.R. (2009). Non-muscle myosin II takes centre stage in cell adhesion and migration. *Nat Rev Mol Cell Biol* 10, 778-790.

Vizcaino, J.A., Csordas, A., del-Toro, N., Dianes, J.A., Griss, J., Lavidas, I., Mayer, G., Perez-Riverol, Y., Reisinger, F., Ternent, T., *et al.* (2016). 2016 update of the PRIDE database and its related tools. *Nucleic Acids Res* 44, D447-456.

Wang, Z., Ahmad, A., Li, Y., Kong, D., Azmi, A.S., Banerjee, S., and Sarkar, F.H. (2010). Emerging roles of PDGF-D signaling pathway in tumor development and progression. *Biochim Biophys Acta* 1806, 122-130.

Weidner, N., Semple, J.P., Welch, W.R., and Folkman, J. (1991). Tumor angiogenesis and metastasis--correlation in invasive breast carcinoma. *The New England journal of medicine* 324, 1-8.

Wieland, E., Rodriguez-Vita, J., Liebler, S.S., Mogler, C., Moll, I., Herberich, S.E., Espinet, E., Herpel, E., Menuchin, A., Chang-Claude, J., *et al.* (2017). Endothelial Notch1 Activity Facilitates Metastasis. *Cancer cell* 31, 355-367.

Wilkes, E.H., Casado, P., Rajeeve, V., and Cutillas, P.R. (2017). Kinase activity ranking using phosphoproteomics data (KARP) quantifies the contribution of protein kinases to the regulation of cell viability. *Mol Cell Proteomics* 16, 1694-1704.

Wong, P.P., Demircioglu, F., Ghazaly, E., Alrawashdeh, W., Stratford, M.R., Scudamore, C.L., Cereser, B., Crnogorac-Jurcevic, T., McDonald, S., Elia, G., *et al.* (2015). Dual-action combination therapy enhances angiogenesis while reducing tumor growth and spread. *Cancer cell* 27, 123-137.

Xian, X., Hakansson, J., Stahlberg, A., Lindblom, P., Betsholtz, C., Gerhardt, H., and Semb, H. (2006). Pericytes limit tumor cell metastasis. *J Clin Invest* 116, 642-651.

Xing, Y., Zhao, S., Zhou, B.P., and Mi, J. (2015). Metabolic reprogramming of the tumour microenvironment. *FEBS J* 282, 3892-3898.

Yonenaga, Y., Mori, A., Onodera, H., Yasuda, S., Oe, H., Fujimoto, A., Tachibana, T., and Imamura, M. (2005). Absence of smooth muscle actin-positive pericyte coverage of tumor vessels correlates with hematogenous metastasis and prognosis of colorectal cancer patients. *Oncology* 69, 159-166.

You, W.K., Yotsumoto, F., Sakimura, K., Adams, R.H., and Stallcup, W.B. (2014). NG2 proteoglycan promotes tumor vascularization via integrin-dependent effects on pericyte function. *Angiogenesis* 17, 61-76.

FIGURE LEGENDS

Figure 1. High percentages of tumor blood vessels that are mural- β 3-integrin negative correlate with increased tumor size and enhanced disease progression in human cancers. (A) Human cutaneous melanoma (n=53), human diffuse large B-cell lymphoma (DLCL) (n=54) and human breast cancer (n=80) sections double-immunostained for β 3-integrin and α -SMA. Representative images of melanoma sections. Arrows, β 3-integrin negative blood vessels. Bar charts, % of blood vessels that are mural β 3-integrin negative for individual patients. (B) Violin plots, individual tumor size. (C) CD31 immunostaining and blood vessel density. (D) In cutaneous melanoma patients, more than the mean % (>41%) of tumor blood vessels that are mural- β 3-integrin negative associated significantly with increased metastasis incidence (n=50 patient samples). (E) In human lymphoma, more than the mean (49%) percentage of mural- β 3-integrin negative tumor blood vessels (tumor blood vessels that are mural- β 3-integrin negative) stratified tumors with advanced disease (stages II-IV) (n=103 patient samples). (F) Breast cancer patients with more than the mean % (57%) of tumor blood vessels that are mural- β 3-integrin negative stratified into those with an increase in relapse incidence (n=63 tumor samples). (G) In human mesothelioma, a high percentage of mural- β 3-integrin negative blood vessels (>51% of tumor blood vessels that are mural- β 3-integrin negative) significantly stratified those with advanced, aggressive types of mesothelioma including biphasic and sarcomatoid mesothelioma (n=22 patient samples). Each sample on the violin plots represent individual patient data. Means \pm S.E.M are given. **p < 0.01, ***p < 0.001. N.S., no significant difference. Scale bar in (A) 25 μ m. (B, C, E, G) Student's *t* test. (D, F) Chi-square test.

Figure 2, Pericyte- β 3-integrin-deletion increases tumor growth. (A) Double immunofluorescence staining for β 3-integrin in B16F0 subcutaneous tumours in *pdgfr β cre+; β 3^{fl/fl}* and *pdgfr β cre-; β 3^{fl/fl}* mice. (B) B16F0 and (C) LLC tumor growth in *pdgfr β cre+; β 3^{fl/fl}* and *pdgfr β cre-; β 3^{fl/fl}* mice (n=10-14 mice per group). Representative images of B16F0 and LLC tumors are given. (D, E) *Pdgfr β cre-; β 3^{fl/fl}* and *pdgfr β cre+; β 3^{fl/fl}* mice were injected with either B16F10 melanoma (D) or LLC cells (E) via the tail vein. Representative high-resolution microCT images of lung capacity 16 days post tumor cell inoculation are given. Red signal represents air in lungs. Graphs represent lung capacity and % loss of lung capacity (n=4-5 mice imaged per group). (F, G) Loss of pericyte β 3-integrin expression significantly increased the number and size of lung nodules in both B16F10 (F) and LLC (G). Bar charts represent means \pm s.e.m. (n=7-9 mice per group). Representative images of tumor burdened lungs and their hematoxylin and eosin (H&E)-stained sections are given. (H) Orthotopic E0771 tumour growth. (n=6 mice/group). (I) Tumor size in 13 week old *RIPtag-2; pdgfr β cre+; β 3^{fl/fl}* and *RIPtag-2; pdgfr β cre-; β 3^{fl/fl}* mice (n=8-10 mice per group). H&E of pancreatic tumor sections provided. *p < 0.05, **p < 0.01, ***p < 0.001. (B-E, H) Two-way ANOVA test. (F-G, I) Student's

t test. Scale bars in (A) 10 μ m, (B-E) 5 mm, (F, G) gross lung, 1.0 cm, H&E sections, 500 μ m, (I) 200 μ m.

Figure 3. Tumor blood vessel density, perfusion, pericyte coverage, leakage and blood flow are not affected by pericyte- β 3-integrin-loss. Midline sections of (A) B16F0 subcutaneous tumors and (B) primary *RIPtag-2* tumors immunostained for endomucin to detect blood vessels (n=4 mice/group) or double immunostained for endomucin and α -SMA for % pericyte-free vessel analysis. (C) Mice injected antemortem via the tail vein with a PE-PECAM antibody (red) to detect perfused blood vessels. Tumor sections subsequently immunostained for endomucin to detect all blood vessels (green) and the % of perfused blood vessel assessed by counting the % of endomucin positive blood vessels that displayed PE-PECAM. (n=3-5 tumors/group). (D) Tumour sections double immunostained for basement membrane marker collagen IV (green) and CD31 (red). Bar charts, percentage of blood vessels with associated collagen IV expression (n=9-10 B16F0 tumors/group) (n=4 *RIPtag-2* tumors/group). (E) For blood vessel leakage mice were injected via the tail vein, in an antemortem process, with PE-PECAM ab (red) and Hoechst dye (blue). Relative area of Hoechst dye uptake into perivascular tumor cells to area of PE-PECAM provides an indication of vessel leakage. Bar charts, means \pm s.e.m. (n=4-5 tumors analyzed per group). (F) Doppler ultrasonography in live mice provides relative blood flow, tumor perfusion, and tumor blood volume in subcutaneous B16F0 tumors. Representative ultrasound images. Bar charts, quantitation across the whole tumors (n=4-5 tumors analyzed per group). N.S., no significant difference. (A-F) Student's *t* test. Scale bars in (A-C) 50 μ m, (D) 10 μ m, (E) 25 μ m and (F) 5 mm.

Figure 4. β 3-integrin deficient pericytes enhance tumor cell growth independent of the tumor vasculature. (A) Tumour growth in WT mice injected subcutaneously with either B16F0 cells plus WT pericytes, or B16F0 plus β 3-null pericytes at 1:8 ratios. (n=10 tumors/group). (B) Blood vessel density and the percentage of vessels without associated α -SMA positive pericyte coverage (n=10 tumors/group). (C) B16F10 tumor growth in lungs of wildtype mice injected via the tail vein with either B16F10 cells plus WT pericytes or B16F10 cells plus β 3-null pericytes at 1:4 or 1:8 ratios at 21 days post injection. Gross tumor burdened lungs and H&E stained images are given (n=3-5 mice/group). (D) WT mice injected with either 0.5×10^6 CMTPIX labelled WT pericytes or β 3-null pericytes and lungs harvested at 2 h and 48 h after the injection. Representative stereomicroscopic images of fresh lungs from both genotypes (n=4-5 lungs per group). (E) Quantitation showed no difference in blood vessel density across any of the groups (detailed in C). Bar charts, means \pm s.e.m. (n=3-5 tumor burdened lungs analyzed per group). (F) Transwell cell invasion assay showed no significant difference in invasion between B16F0 cells treated with conditioned medium from either WT pericytes or β 3-null pericytes (n=9-11 technical repeats). (G) E0771 cells were co-injected with WT- or β 3-null pericytes into the

mammary fat pad of C75BL/6 mice. Mice were culled when tumors reached 600 mm³ and lung metastases assessed (n= 8-9 mice/group). Representative images of H&E stained sections are given. (H) Conditioned medium from WT or β 3-null pericytes was applied to B16F0, B16F10 and LLC cells and cell survival measured by MTS assays. Results are means \pm s.e.m. relative to tumor cells treated with conditioned media from WT pericytes (n= 3 experimental repeats). *p < 0.05, **p < 0.01, ***p < 0.001. N.S., no significant difference. PC, pericytes. (A) Two-way ANOVA test. (B-H) Student's *t* test. Scale bars in (B, G) 50 μ m, (C) gross lung, 1.0 cm, and H&E sections, 100 μ m, (D) 500 μ m, (G) 50 μ m.

Figure 5, Loss of pericyte- β 3-integrin expression significantly increases FAK-pHGFR-pAkt-p-p65 dependent cytokine production. (A) Volcano plots of phosphoproteomic analysis shows significant enhancement of several phosphoproteins including FAK in β 3-null vs WT pericytes. (B) Analysis of receptor tyrosine kinase (RTK) arrays or tyrosine kinase (TK) arrays shows a significant increase in p-HGFR, p-Akt (S473) and p-Akt (T308) levels in β 3-null pericytes compared with WT pericytes (n= 4 dots from 2 experimental repeats). (C) Western blot analysis of WT and β 3-null pericyte lysates. Bar charts represent densitometric values \pm s.e.m (n=3 experimental repeats). Hsc70, loading control. (D) *Protein-profiler* cytokine array analysis of fold increase in cytokine expression between WT and β 3-null pericytes (n=4 dots from 2 experimental repeats). Representative images of the relevant dots from the cytokine arrays are given. Human cutaneous melanoma, lymphoma and ER+ breast cancer samples were double immunostained for the mural cell marker α -SMA and for either p-Akt (E) or nuclear p65 (F). High proportions of mural- β 3-integrin negative blood vessels is associated with elevated levels of p-Akt and nuclear p65 in all human cancers (n=5-6 patient samples). Representative images of double immunostained sections from each cancer type for α -SMA and with either p-Akt or p65 are given. Arrows highlight p-Akt (E) or nuclear p65 (F) staining. Each sample in the violin plots given represents individual tumors from separate patients. Means \pm S.E.M are given. (G) Western blot analysis of β 3-null pericytes after treatment with vehicle alone (DMSO) or FAK inhibitor (PF573228 10 μ M). Blots are representative of 3 separate experiments. β 3-null pericytes were treated with either vehicle alone (DMSO), HGFR-inhibitor (H) or Akt-inhibitor (I) for 10, 30 and 60 minutes. Western blot analysis of DMSO, HGFR-inhibitor or Akt-inhibitor treated β 3-null pericytes. Bar charts represent means \pm s.e.m. (n=3 experimental repeats). *p < 0.05, **p < 0.01, ***p < 0.001. (B-I) Student's *t* test. Scale bars in (E, F) 10 μ m.

Figure 6, Deletion of pericyte- β 3-integrin enhances tumor cell growth via pericyte-pAkt-p65 regulated cytokine production. (A) Western blot analysis of β 3-null pericytes with CRISPR-Cas9 deletion of Akt1 (β 3-null;Akt^{KO} PC) or HGFR (β 3-null;HGFR^{KO} PC) compared

with $\beta 3$ -null;Cas9 controls. Hsc70, loading control. Blots representative of 3 separate experiments. (B) B16F0 cell survival after exposure to conditioned media from $\beta 3$ -null;Akt^{KO}, $\beta 3$ -null;HGFR^{KO}, or $\beta 3$ -null;Cas9 pericytes (n= 16 technical replicates for 2 separate experiments). (C) Tumor growth in WT mice injected subcutaneously with either B16F0 cells plus $\beta 3$ -null;Cas9 pericytes or B16F0 plus $\beta 3$ -null;Akt^{KO} pericytes at 1:8 ratio. (D) Western blot analysis using mock- and I κ -B α -SR-transfected WT or $\beta 3$ -null pericyte lysates. HSC70, loading control. (E) *Protein-profiler* cytokine arrays. Quantitation of fold difference in cytokine expression between mock- and I κ -B α -SR-transfected $\beta 3$ -null pericytes (n=4 dots from 2 independent experiments). (F) Conditioned media from mock- and I κ -B α -SR-transfected $\beta 3$ -null pericytes were applied to B16F0, B16F10 and LLC cells and cell survival measured by MTS assay. Bar charts, means \pm s.e.m. relative to tumor cells treated with conditioned media from mock-transfected $\beta 3$ -null pericytes (n=3 experimental repeats). (G) Wild type mice were injected via the tail vein with either B16F10 cells and mock-transfected $\beta 3$ -null pericytes or B16F10 cells and I κ -B α -SR-transfected $\beta 3$ -null pericytes and lungs harvested for lung nodule analysis at 21 days post injection with representative gross lung and H&E stained sections (n=3 mice/group). Bar charts, means \pm s.e.m. for numbers of lung nodules and sizes of lung nodules across all groups. (H) Western blot confirmed the CRISPR-Cas9 depletion of CXCL1, CCL2 or TIMP-1 in $\beta 3$ -null pericytes back to WT;Cas9 levels. Bar charts, densitometric analysis. (I) MTS cell survival of B16F0 cells exposed to conditioned medium from Cas9-control transfected $\beta 3$ -null pericytes ($\beta 3$ -null;Cas9), or CRISPR-knockout CXCL1, TIMP-1 or CCL2 $\beta 3$ -null pericytes (namely, $\beta 3$ -null;CXCL1^{KO}, $\beta 3$ -null;TIMP-1^{KO}, $\beta 3$ -null;CCL2^{KO} respectively). Results are means \pm s.e.m. relative to tumor cells treated with conditioned media from $\beta 3$ -null;Cas9. (J) Tumour growth in WT mice injected subcutaneously with either B16F0 cells plus $\beta 3$ -null;Cas9 pericytes, or B16F0 plus $\beta 3$ -null;CXCL1^{KO}, $\beta 3$ -null;TIMP-1^{KO}, or $\beta 3$ -null;CCL2^{KO} pericytes. Bar charts, means \pm s.e.m. *p < 0.05, **p < 0.01, ***p < 0.001. N.S., no significant difference. (B, E-G, I) Student's *t* test. (C, J) Two-way ANOVA test. Scale bar in (G) gross lung, 1.0 cm, and H&E sections, 100 μ m

Figure 7, Deletion of pericyte- $\beta 3$ -integrin increases tumor cell growth via pericyte-CCL2 and tumor cell-MEK1 and ROCK2 pathways.

(A) KSEA analysis of phosphoproteomics identifies kinase substrate pathway enrichment in B16F0 cells exposed to conditioned medium from $\beta 3$ -null pericytes compared with B16F0 cells exposed to conditioned medium from WT pericytes. (B) Phospho-MLC2 immunohistochemical staining, and signal intensity maps. Bar chart, H-score of mean signal intensity \pm s.e.m. in B16F0 tumors co-injected with WT or $\beta 3$ -null pericytes. (C) Western blot analysis in B16F0 cells exposed to conditioned medium from $\beta 3$ -null;Cas9 or $\beta 3$ -null;CCL2^{KO} pericytes. Blots are representative of 3 separate experiments. (D) Phospho-MLC2 staining and intensity maps in B16F0 tumors co-injected with WT;Cas9, $\beta 3$ -null;Cas9 or $\beta 3$ -null;CCL2^{KO} pericytes. Bar chart, H-score of mean signal intensity \pm s.e.m. (E) Western blot analysis of B16F0 cells treated with

MEK1 inhibitor U0126 indicating inhibition of the MEK effector ERK1/2, and of p-MLC2 in B16F0 cells treated with the ROCK2 inhibitor GSK269962A indicating inhibition of activity of the ROCK effector MLC2. **(F)** B16F0 cells were exposed to conditioned medium from WT or $\beta 3$ -null pericytes in combination with either vehicle, MEK1 inhibitor, U0126 or ROCK2 inhibitor, GSK269962A and B16F0 cell survival measured in MTS assay. **(G)** B16F0;ROCK2^{KO} and B16F0;ROCK2^{WT} cells were injected subcutaneously into *pdgfr β cre-;* $\beta 3^{fl/fl}$ and *pdgfr β cre+;* $\beta 3^{fl/fl}$ mice. Once tumors were established, mice were treated with doxycycline to induce ROCK2 deletion in B16F0 cells *in vivo* (n= 5-9 mice per group). *Line graph*, tumor growth, *bar chart*, mean end tumor volume \pm s.e.m. *p < 0.05, ***p < 0.001. N.S., no significant difference. **(B, D, F, G, Bar chart)** Student's *t* test. **(G, line graph)** Two-way ANOVA test. Scale bar in **(B, C)** 100 μ m.

KEY RESOURCES TABLE

REAGENT or RESOURCE	SOURCE	IDENTIFIER
Antibodies		
Mouse monoclonal anti-HGFR (Met)	Santa Cruz Biotechnology	CAT#sc-8057; RRID:AB_673755
Rabbit monoclonal anti-phospho-HGFR (Met)	Cell Signaling Technology	CAT#3077;RRID:AB_2143884
Rat monoclonal anti-endomucin	Santa Cruz Biotechnology	CAT#sc-65495;RRID:AB_2100037
Rabbit monoclonal anti- β 3-integrin	Cell Signaling Technology	CAT#4702;RRID:AB_2296320
Rabbit monoclonal anti- β 5-integrin	Cell Signaling Technology	CAT#3629;RRID:AB_2249358
Rabbit monoclonal anti- β 1-integrin	Cell Signaling Technology	CAT#4706;RRID:AB_823544
Rabbit monoclonal anti-PDGFR β	Cell Signaling Technology	CAT#3169;RRID:AB_AB_2162497
Rabbit polyclonal anti-NG2	Merck-Millipore	CAT#AB5320;RRID:AB_11213678
Rabbit monoclonal anti-NF- κ B p65	Cell Signaling Technology	CAT#8242;RRID:10859369
Rabbit monoclonal anti-phospho-NF- κ B p65	Cell Signaling Technology	CAT#3033; RRID:AB_331285
Rabbit monoclonal anti-Akt	Cell Signaling Technology	CAT#4691; RRID:AB_915783
Rabbit monoclonal anti-phospho-Akt	Cell Signaling Technology	CAT#4060;RRID:AB_2315049
Mouse monoclonal anti-Hsc70	Santa Cruz Biotechnology	CAT#sc7298; RRID:AB_627761
Goat polyclonal anti-MCP-1 (CCL2)	ThermoFisher Scientific	CAT#PA5-46954; RRID:AB_2609536
Rat monoclonal anti-CXCL1	ThermoFisher Scientific	CAT#MA5-23811;RRID:AB_2609587
Mouse monoclonal anti-TIMP-1	ThermoFisher Scientific	CAT#MA5-13688;RRID:AB_11004132
Rabbit monoclonal anti-Myosin Light Chain 2 (MLC2)	Cell Signaling Technology	CAT#3672;RRID:AB_10692513
Rabbit monoclonal anti-phospho-Myosin Light Chain 2	Cell Signaling Technology	CAT#3674;RRID:AB_2147464
Rabbit monoclonal anti-phospho-Myosin Light Chain 2	Cell Signaling Technology	CAT#3671;RRID:AB_330248
Rabbit polyclonal anti-phospho-FAK (Tyr397)	Cell Signaling Technology	CAT#3283;RRID:AB_2173659
Mouse monoclonal anti-Akt1	Cell Signaling Technology	CAT#2967;RRID:AB_331160
Rabbit polyclonal anti-phospho-MEK1/2	Cell Signaling Technology	CAT#9121;RRID:AB_331648
Mouse monoclonal anti-ROCK II	Biosciences	CAT#610624;RRID:AB_397956

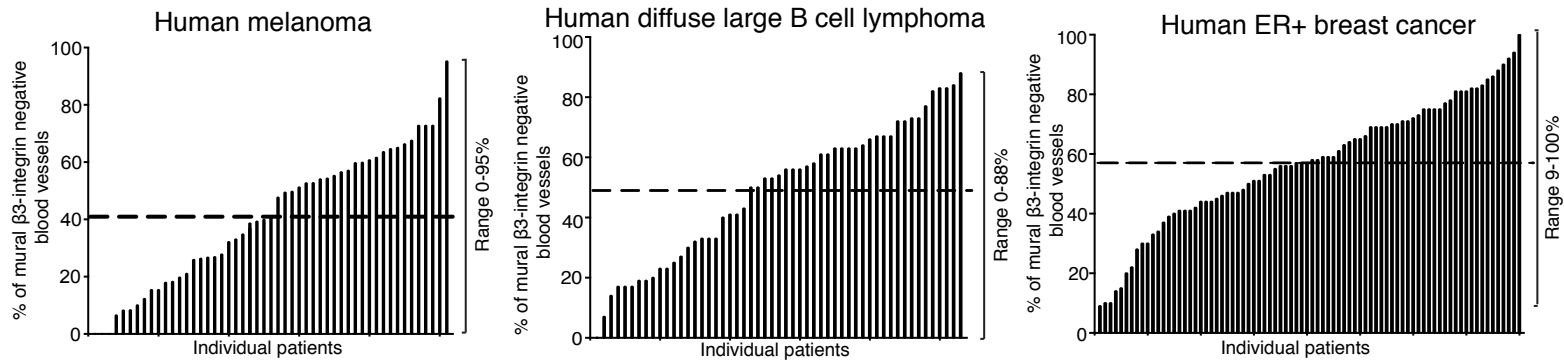
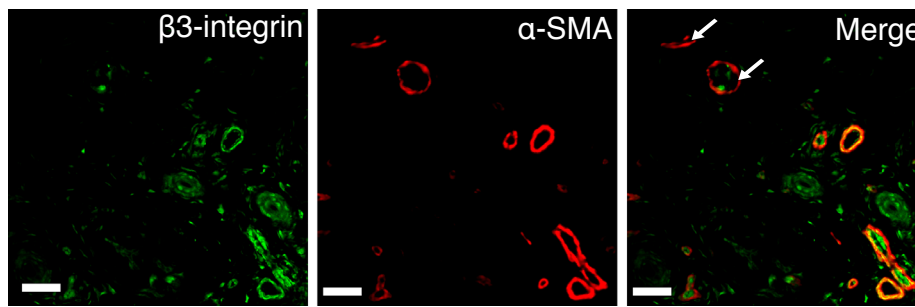
Rabbit polyclonal anti-NG2, Alex Fluor®488 conjugated	Merck-Millipore	CAT#AB5320A4;RRID:AB_11203143
Rat monoclonal PE anti-mouse CD31	BioLegend	CAT#102408;RRID:AB_312903
Rat monoclonal PE anti-mouse/human CD11b (Mac1)	BioLegend	CAT#101208;RRID:AB_312791
Rat monoclonal APC-anti-mouse CD140b (PDGFR β)	BioLegend	CAT#136008;RRID:AB_2268091
Rat monoclonal APC-anti-mouse CD140a (PDGFR α)	BioLegend	CAT#135908;RRID:AB_2043970
Rat monoclonal PE/Cy7-anti-mouse CD146	BioLegend	CAT#134714;RRID:AB_2563109
Rabbit polyclonal anti-collagen IV	Abcam	CAT#ab6586;RRID:AB_305584
Rabbit polyclonal anti-CD61 (β 3-integrin)	ThermoFisher Scientific	CAT#PA5-32890;RRID:AB_2550351
Rabbit monoclonal anti- β 3-integrin	Abcam	CAT#ab75872;RRID:AB_2249317
Mouse monoclonal anti-alpha-smooth muscle actin Cy3 conjugated	Sigma-Aldrich	CAT#C6198;RRID:AB_476856
Rat monoclonal anti-mouse FC γ sort-RII/III	BD Biosciences	CAT#553141;RRID:AB_394656
Rat monoclonal anti-mouse ICAM-2	BD Biosciences	CAT#553326;RRID:AB_394784
Goat anti-Rabbit IgG (H+L) Highly Cross-Adsorbed Secondary Antibody, Alexa Fluor® 546 Conjugated	ThermoFisher Scientific	CAT#A-11035;RRID:AB_143051
Goat anti-Rabbit IgG (H+L) Highly Cross-Adsorbed Secondary Antibody, Alexa Fluor® 488 Conjugated	ThermoFisher Scientific	CAT#A-11034;RRID:AB_2576217
Donkey anti-Rat IgG (H+L) Highly Cross-Adsorbed Secondary Antibody, Alexa Fluor® 488 Conjugated	ThermoFisher Scientific	CAT#A-21208;RRID:AB_141709
Biotinylated goat anti-rabbit secondary antibody	Vector Laboratories	CAT#BA-1000;RRID:AB_2313606
Bacterial and Virus Strains		
N/A	N/A	N/A
Biological Samples		
Human ER+ breast cancer samples	Barts Cancer Institute Breast Cancer Now tissue Bank	https://www.breastcancer-tissuebank.org/about-tissue-bank
Human melanoma, mesothelioma and diffuse large B-cell lymphoma	Barts Cancer Institute tissue Bank	N/A
Chemicals, Peptides, and Recombinant Proteins		
Prolong™ Gold Anti-Fade Mountant with DAPI	ThermoFisher Scientific	CAT#P36931
Dual Endogenous Enzyme-Blocking Reagent	Dako	CAT#S2003
Citric acid based antigen unmasking solution	Vector Laboratories	CAT#H-3300;RRID:AB_2336226
VECTASTAIN ABC HRP Elite kit	Vector Laboratories	CAT#PK-6100;RRID:AB_2336819

Vector® VIP Peroxidase (HRP) Substrate Kit	Vector Laboratories	CAT#SK-4600;RRID:AB_2336848
OCT	Killik, Bio-Optica, IT	CAT#W01030799
Hoechst dye	Sigma-Aldrich	CAT#B2261
Collagenase type I	Gibco	CAT#17100017
Gelatin	Sigma-Aldrich	CAT#G9136
Fibronectin	Merck-Millipore	CAT#FC010
DYNAL® sheep anti-rat IgG-conjugated magnetic beads	ThermoFisher Scientific	CAT#11035
CellTracker™ Red CMTPX Dye	ThermoFisher Scientific	CAT#C34552
Lipofectamine 2000	ThermoFisher Scientific	CAT#11668019
MegaMix-Blue	MicroZone, Client life science	CAT#2MMB-100
HGFR inhibitor (PHA-665752)	Merck	CAT#PZ0147-25MG
Akt inhibitor (LY294002)	Merck	CAT#L9908
FAK inhibitor (PF573228)	TORCIS	CAT#3239
ROCK inhibitor (GSK269962A)	TORCIS	CAT#4009
MEK inhibitor (U0126)	TORCIS	CAT#1144
CCR2 inhibitor (CCR2i)	ChemoCentryx	Patent Application Numbers: WO 2014089495 and WO 2016187393
Critical Commercial Assays		
Hypoxyprome™-1 Kit	Hypoxyprome, Inc	CAT#HP1-1000Kit
Tyramide SuperBoost™ Kit	ThermoFisher Scientific	CAT#B40953
Vevo Micromarker™ Contrast Agent Kit	Visualsonics	N/A
CellTiter 96® Aqueous One Solution Reagent	Promega	CAT#G3582
Proteome-Profiler Mouse Cytokine Array Kit	R&D systems	CAT#ARY006
Proteome Profiler Phospho-Receptor Tyrosine Kinase Array Kit	R&D systems	CAT#ARY001B
Proteome Profiler Tyrosine Kinase Array Kit	R&D systems	CAT#ARY003B
Deposited Data		
Mass spectrometry proteomics data	the ProteomeXchange Consortium	PXD014513
Experimental Models: Cell Lines		
LLC	ATCC	CRL-1642
B16F0	ATCC	CRL-6322
B16F10	ATCC	CRL-6475
E0771	CH3 Biosystems	SKU:940001
Experimental Models: Organisms/Strains		
Mouse: <i>pdgfrβcre</i>	Foo et al., 2006	N/A
Mouse: <i>β3^{fl/fl}</i>	Morgan et al., 2010	N/A
Mouse: <i>pdgfrβcre-;β3^{fl/fl}</i>	This paper	N/A
Mouse: <i>pdgfrβcre+;β3^{fl/fl}</i>	This paper	N/A
Mouse: mTmG	Cancer Research UK	N/A
Mouse: <i>pdgfrβcre-;mTmG</i>	This paper	N/A

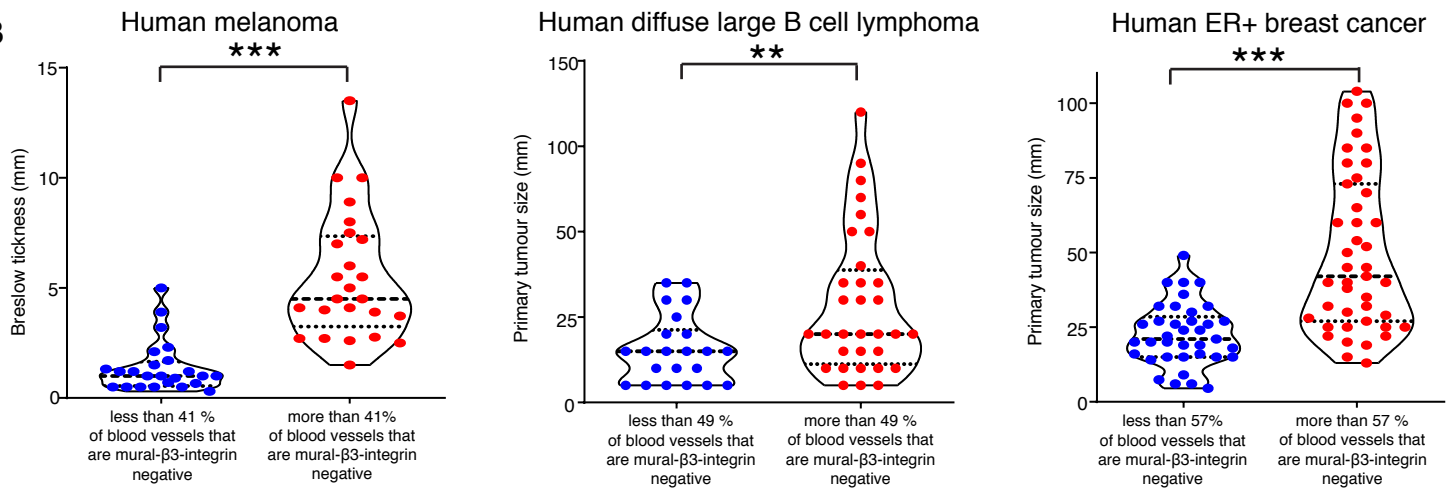
Mouse: <i>pdgfrβcre+;mTmG</i>	This paper	N/A
Mouse: <i>RIPtag-2</i>	Hanahan, 1985	N/A
Mouse: <i>RIPtag-2;pdgfrβcre-;β3^{fl/fl}</i>	This paper	N/A
Mouse: <i>RIPtag-2;pdgfrβcre+;β3^{fl/fl}</i>	This paper	N/A
Oligonucleotides		
PCR primers, see method	This paper	N/A
shRNA sequences for ROCK2 and non-targeting shControl, see method	This paper	GenScript USA Inc.
sgRNAs sequences for TIMP-1, CXCL1, CCL2, Akt1 and HGFR, see table S1	This paper	Invitrogen
Recombinant DNA		
Lenti-CRISPR–EGFP plasmid	Addgene	CAT#75159
pLKO-neo lentiviral shRNA construct	Addgene	CAT#21916
pMDLg/pRRE	Addgene	CAT#12251
pRSV-Rev	Addgene	CAT#12253
pMD2.G	Addgene	CAT#12259
Software and Algorithms		
ImageJ	Schneider et al., 2012	https://imagej.nih.gov/ij/
Graphpad Prism (Version 6 and 8)	Graphpad	http://graphpad.com
Flowjo	N/A	https://www.flowjo.com
QuPath v0.1.2	Quantitative Pathology & Bioimage analysis	https://qupath.github.io/
The RNAi Consortium collection	Sigma-Aldrich	https://www.sigmaaldrich.com/life-science/functional-genomics-and-rnai/shrna/library-information.html
CRISPOR algorithm	Cripsor	http://crispor.tefor.net
Pescal software	Wilkes et al., 2017	N/A
Mascot Daemon 2.5.0	Mascot	N/A
VevoCQ™ contrast quantification software	Visualsonics	N/A
Other		
Nucleofector® electroporation system	Lonza	Nucleofector® II
Neon Transfection system	ThermoFisher Scientific	MPK5000
NanoZoomer S210 slide scanner	Hamamatsu, Japan	S210
FACSAria™ III flow cytometer	BD Biosciences	FACSAria™ III
Nano SPECT/CT® <i>In vivo</i> preclinical imager	BioScan	Nano SPECT/CT®
Ultrasound imaging system	Visualsonics	Vevo® 2100 system
Decloaking Chamber™ NxGen	Biocare Medical	NxGen

Figure 1

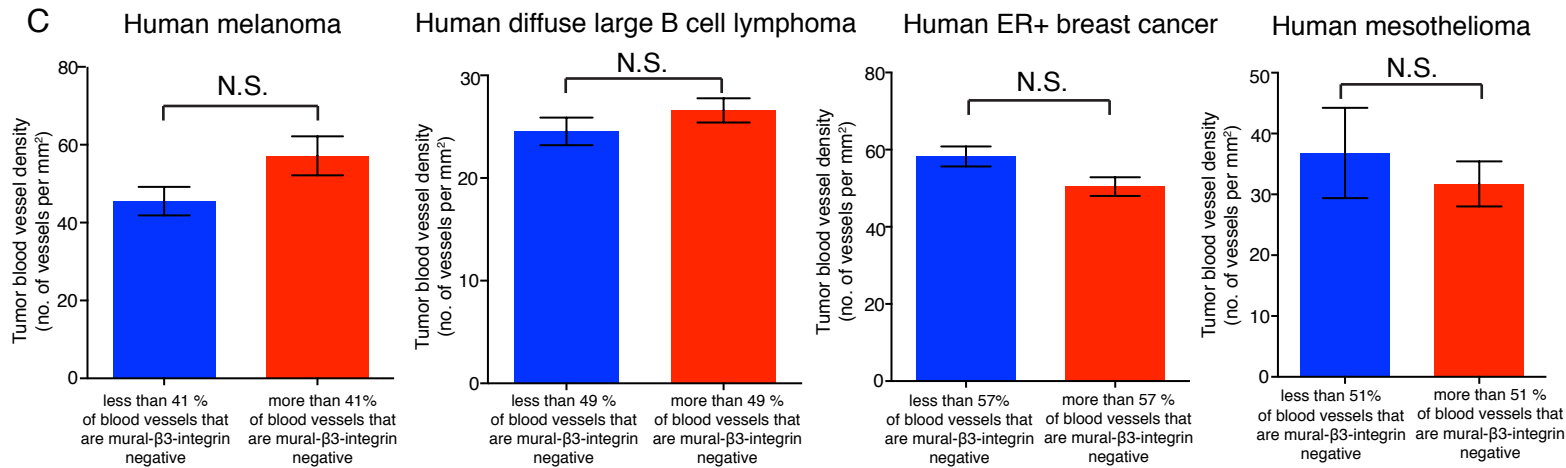
A



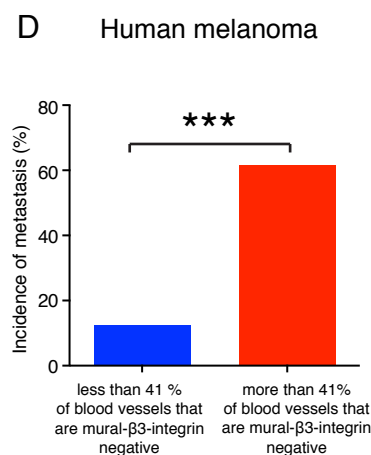
B



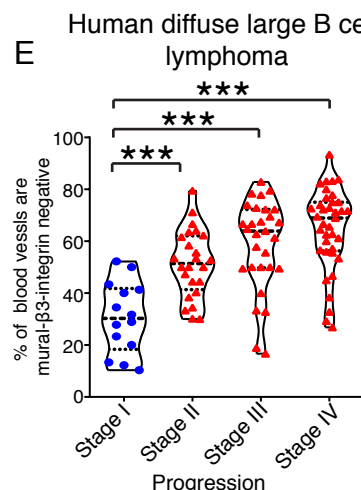
C



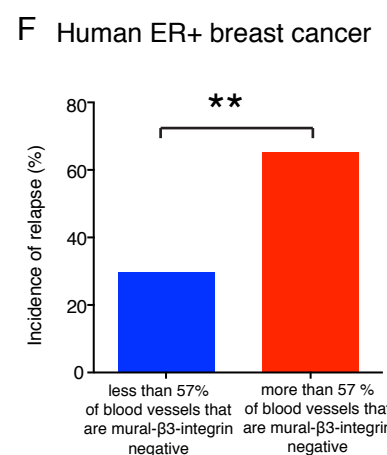
D



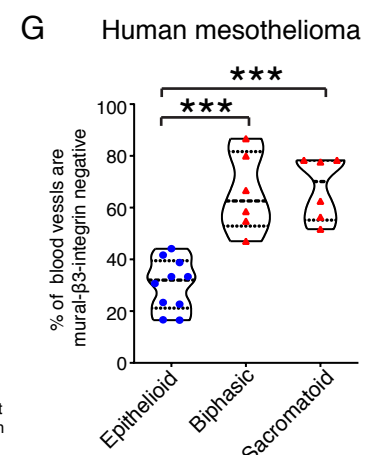
E

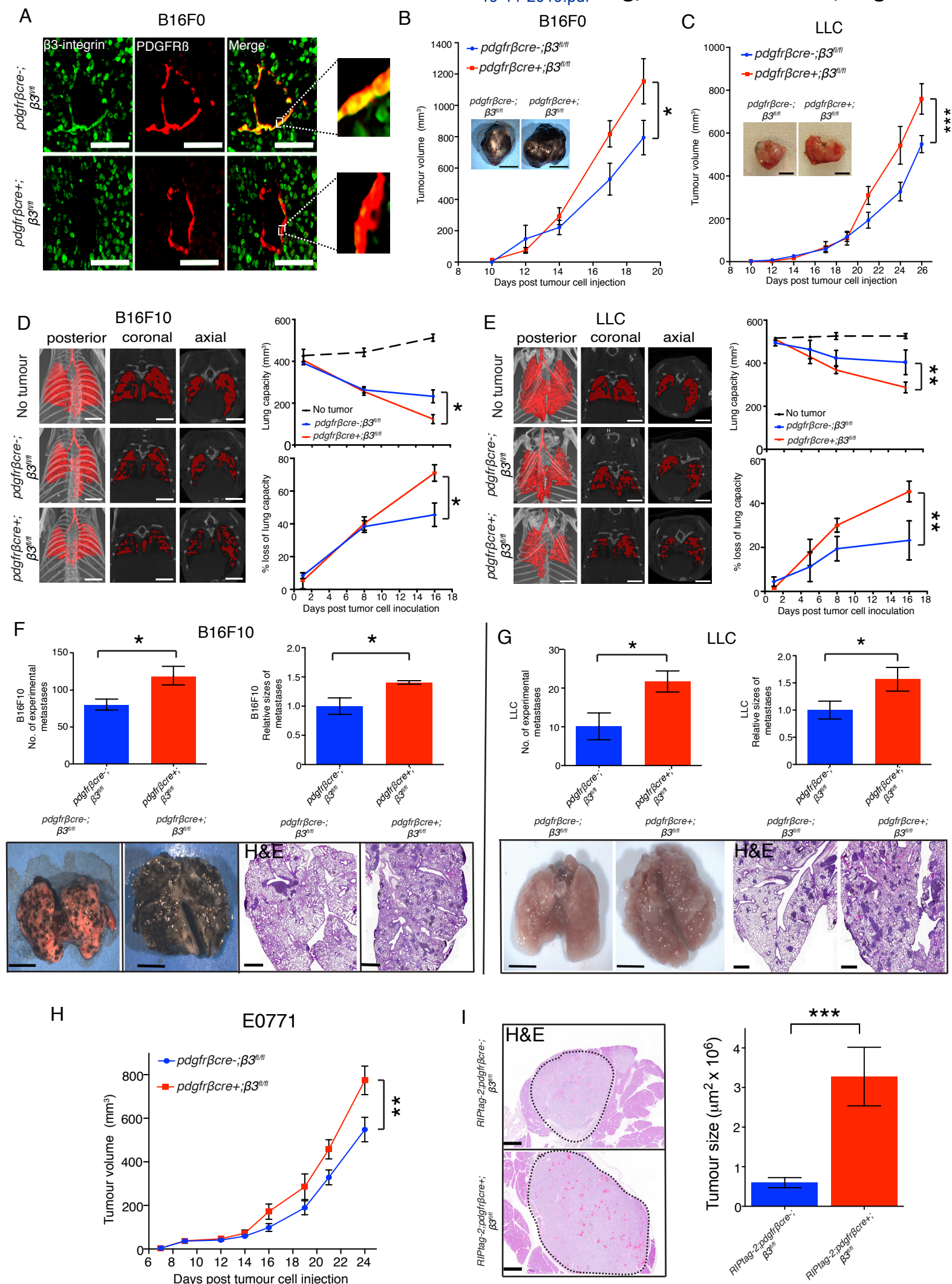


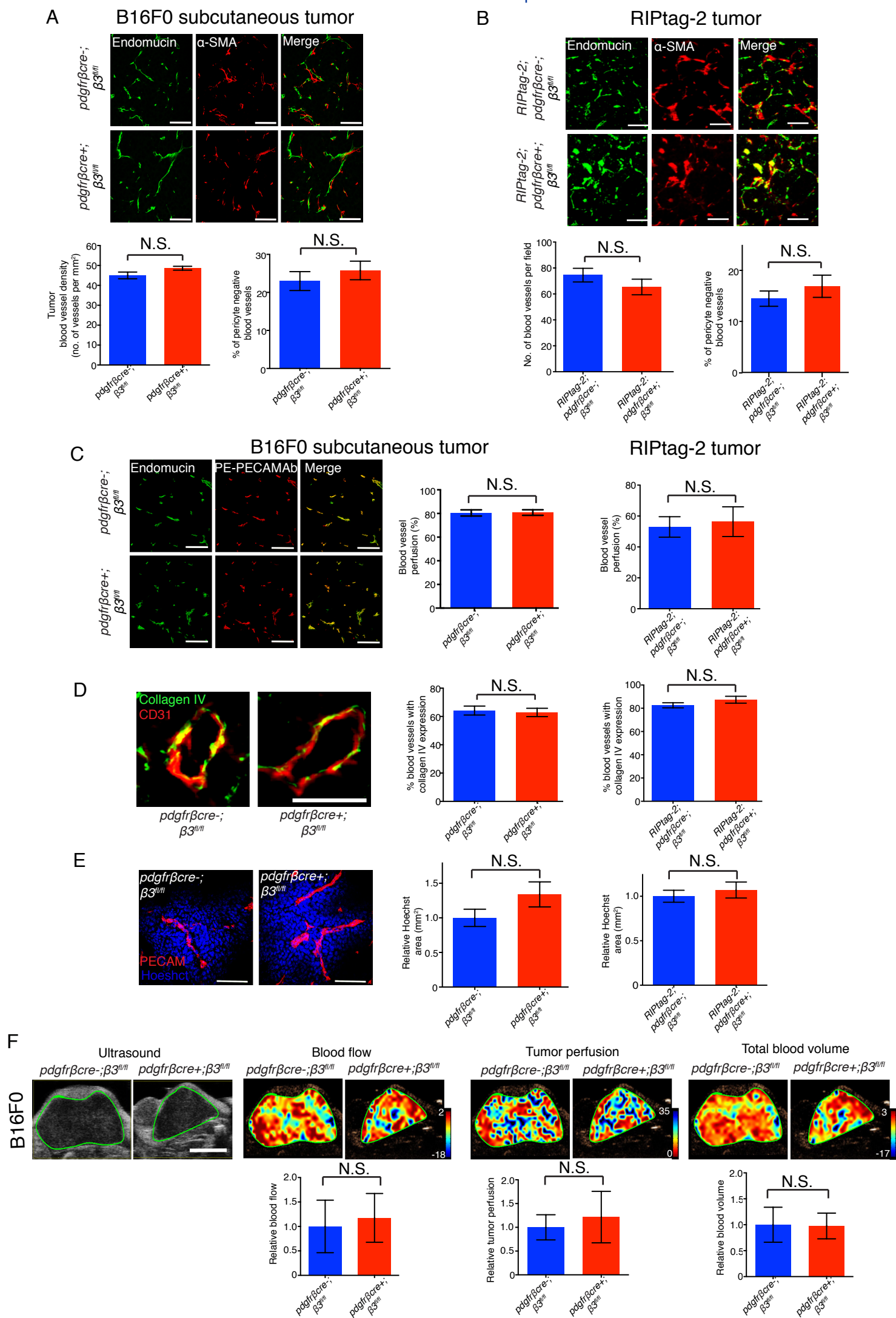
F

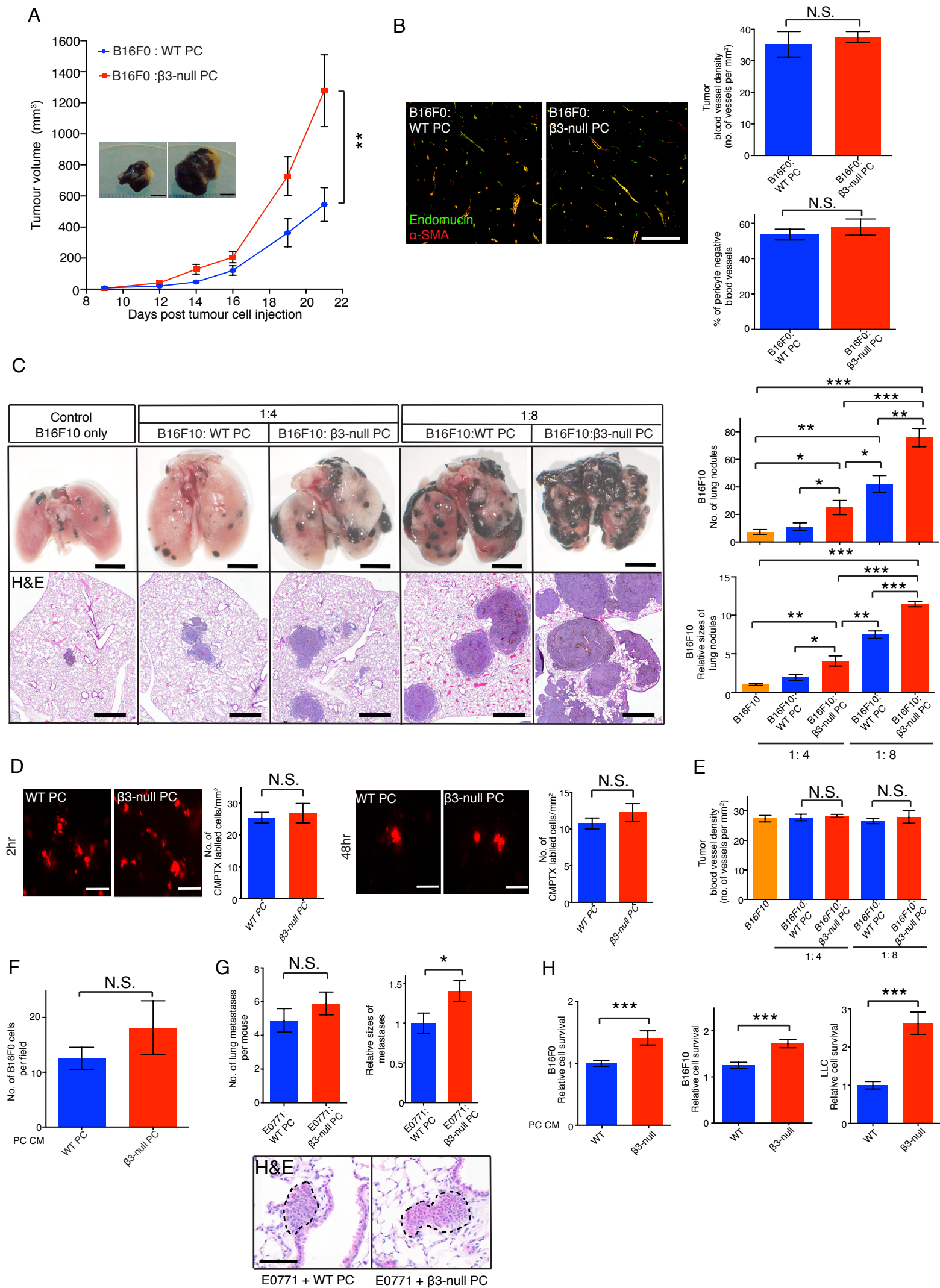


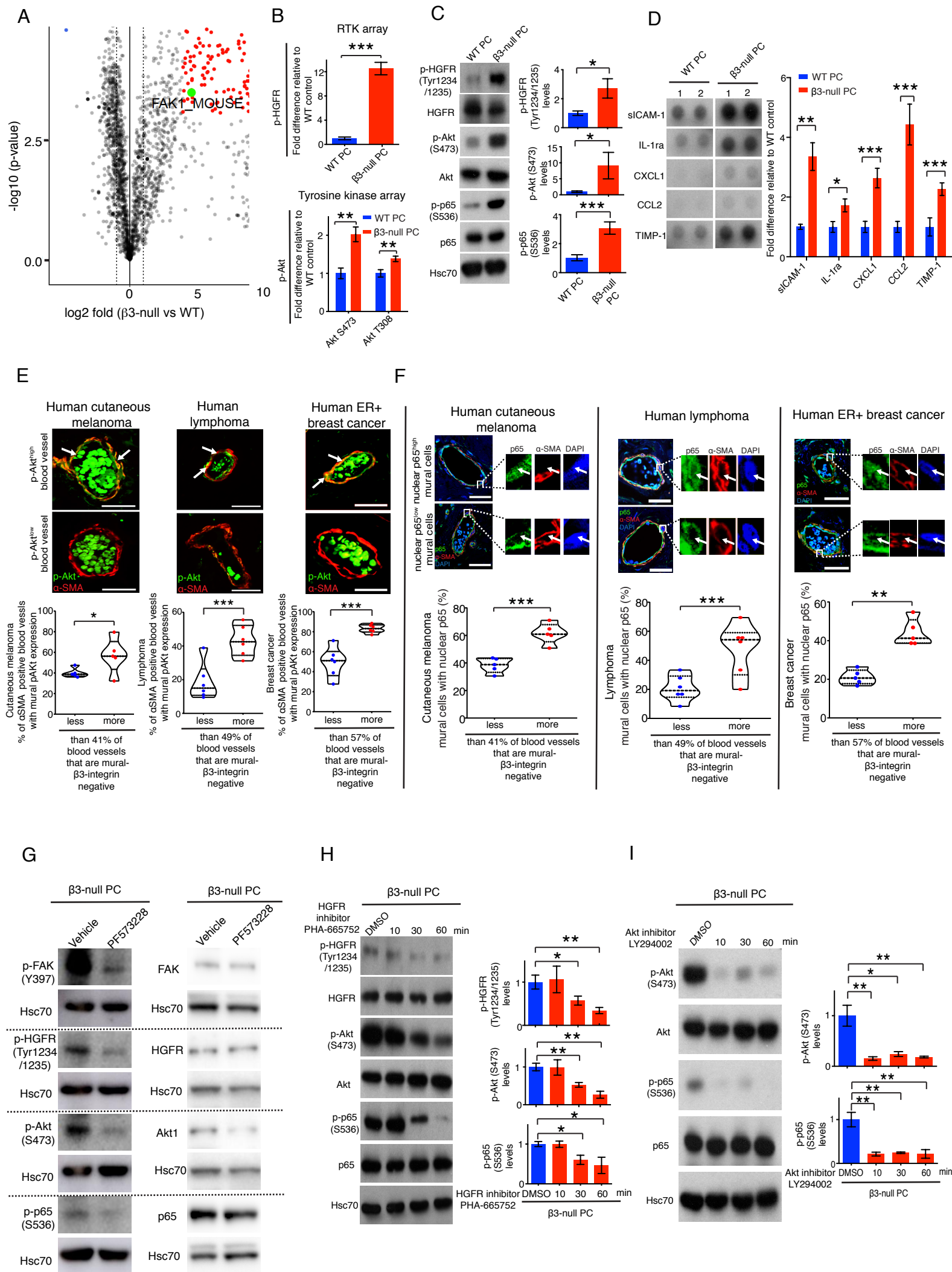
G

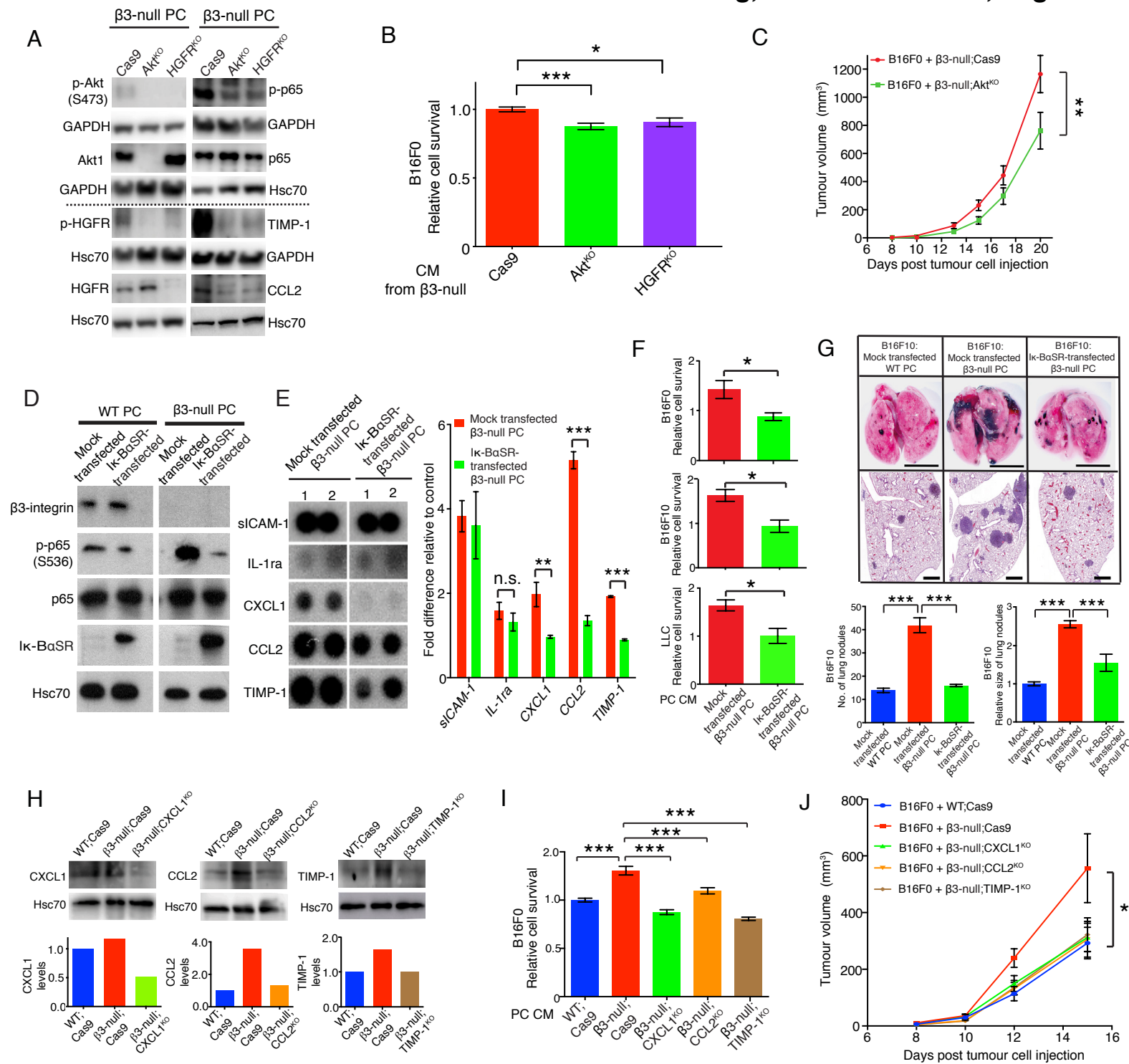










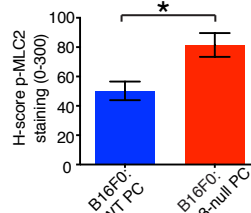
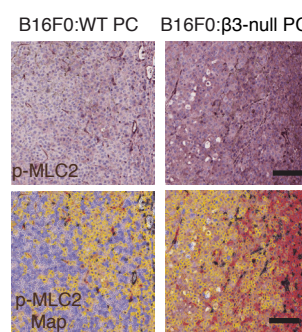
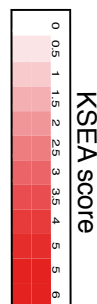


A

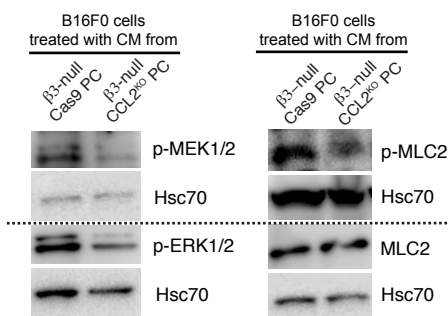
KSEA analysis of B16F0

ROCK2	**	Rdx(T564) Msn(T558) Ezr(T567) Myl12b(S20)
MEK1	***	Mapk1(Y185) Mapk1(T183) Mapk3(Y205) Mapk3(T203)
DAPK1	**	Myl12b(T19) Myl12b(S20)
DAPK3	**	Myl9(T19) Myl9(S20)
smMLCK	**	Myl9(T19) Myl9(S20)
PKCE	*	Prkd1(S748) Stat3(S727)
PKACA	*	Vim(S39) Vim(S7) Mapt(S506) Vim(S51) Arhgef2(S885) Stmn1(S63) Marcks(S163) Marcks(S156) Bad(S136) Ywhah(S59) Crem(S133) Marcks(S152) Bad(S155) Marcks(S160) Stmn1(S16)
Lck	*	Mapk1(Y185)
AurB	*	Vim(S39) Vim(S7)
CDK5	*	Axin1(T480) Cdkn1b(S10) Stat3(S727) Stmn1(S38)
GSK3B	*	Axin1(S485) Axin1(T480) Dpysl2(T514) Map1b(S1260) Zbed3(S111) Rcan1(S112) Rcan1(S108) Myc(T58) Dpysl2(T509) Pax3(S201) Ctnnd1(S252)

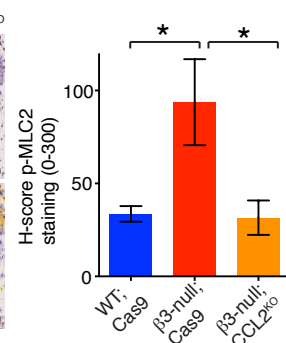
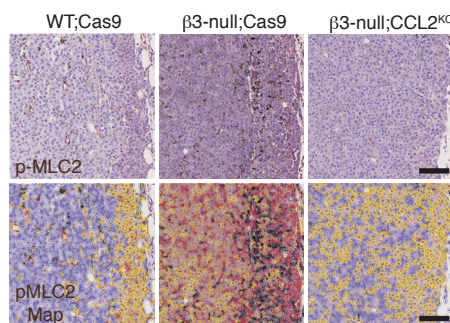
B



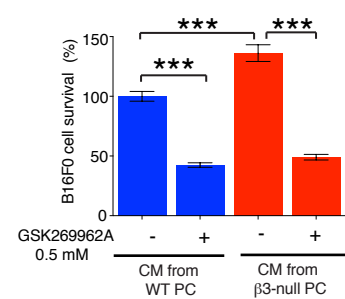
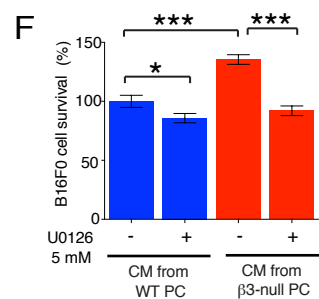
C



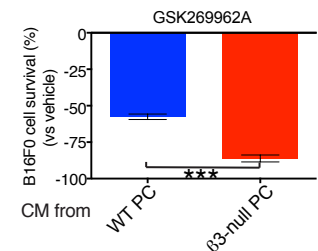
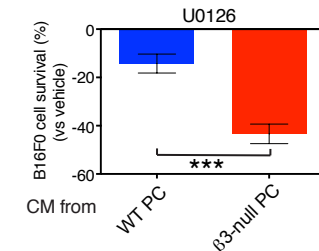
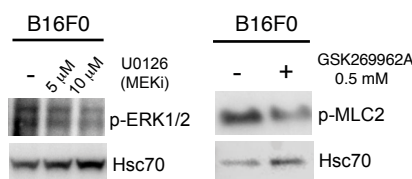
D



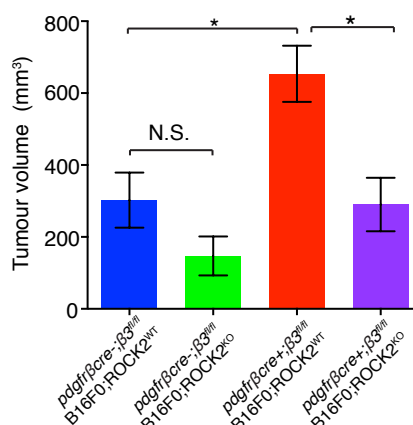
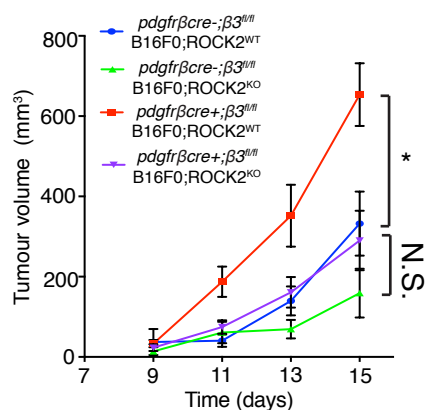
F

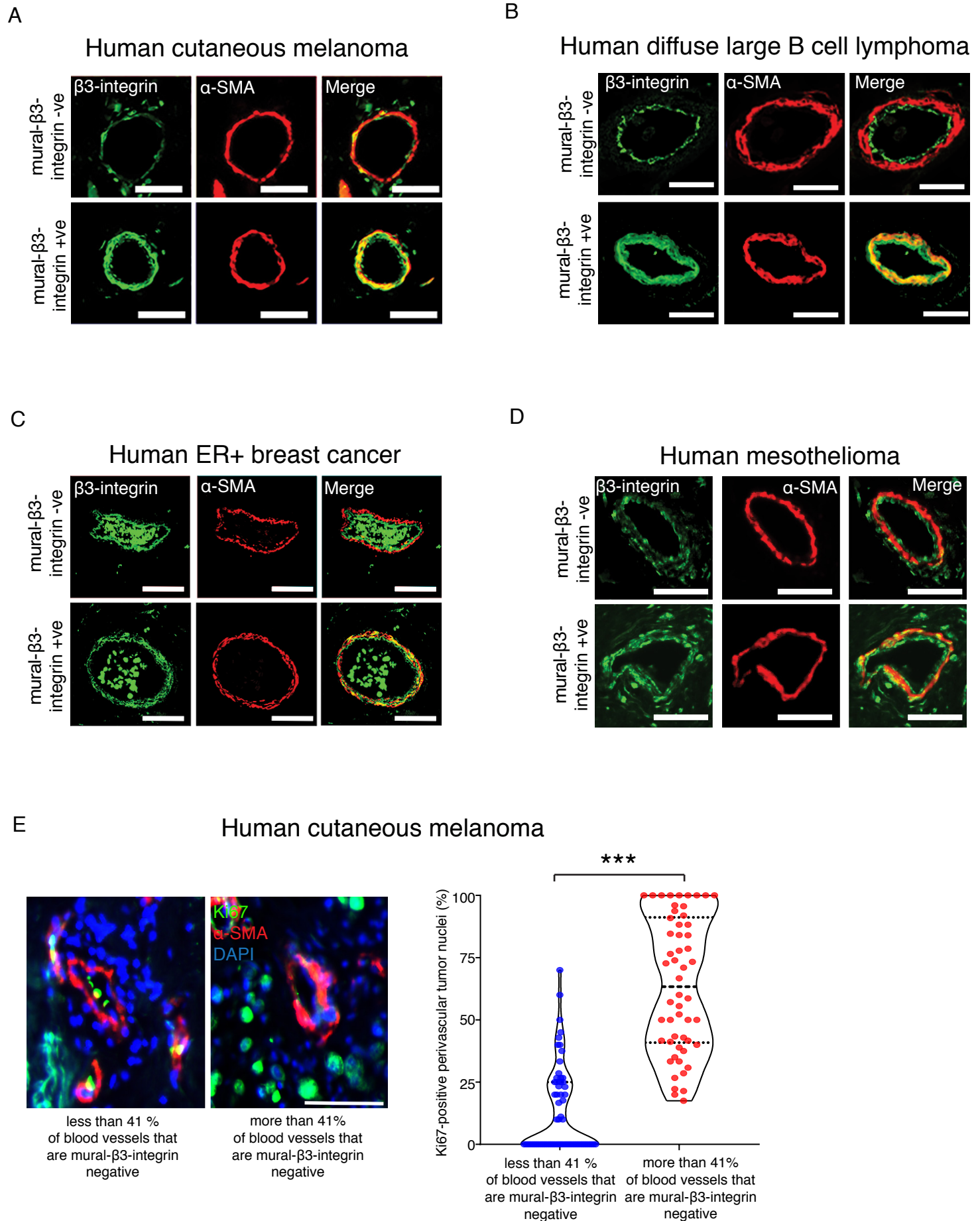


E



G

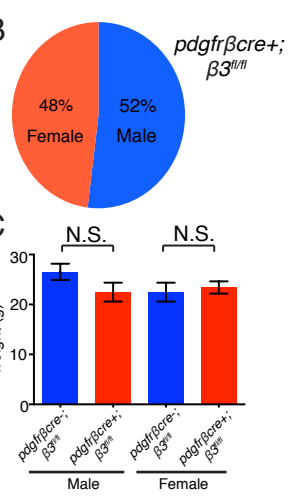




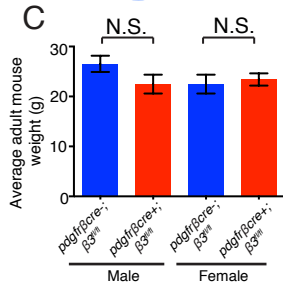
A

Genotype	No. of mice resulting from <i>pdgfrβcre-;</i> <i>β3^{fl/fl}</i> x <i>pdgfrβcre+;</i> <i>β3^{fl/fl}</i>	
	No. of pups	Expressed as %
<i>pdgfrβcre-;</i> <i>β3^{fl/fl}</i>	95	48
<i>pdgfrβcre+;</i> <i>β3^{fl/fl}</i>	100	52

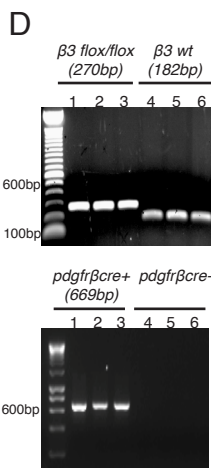
B



C

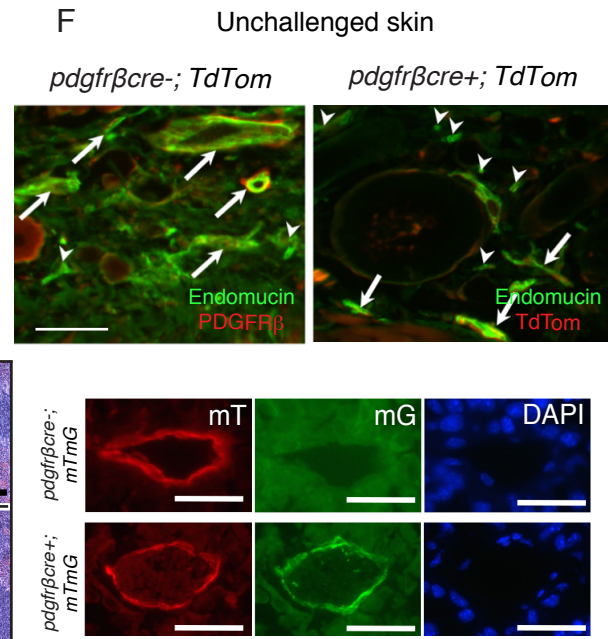


D

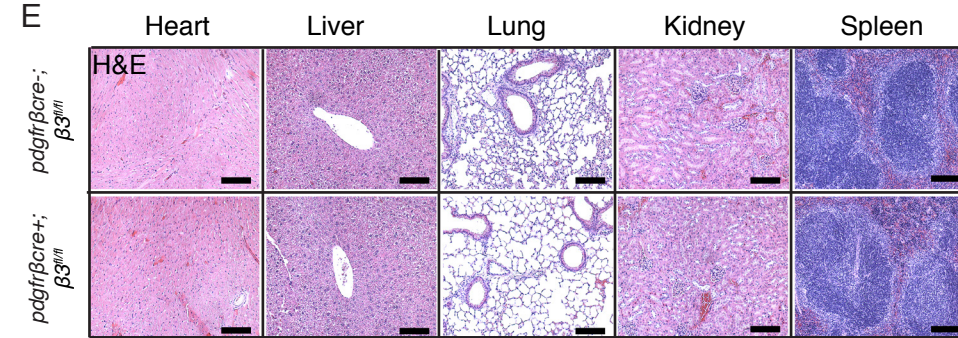


Wong, Muñoz-Félix *et al.*, Supplementary Figure 2 related to Figure 2

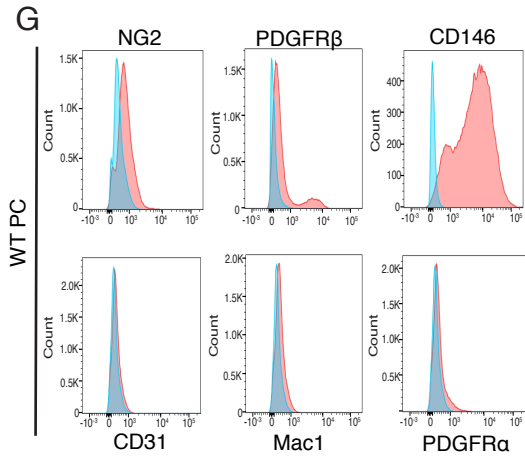
F



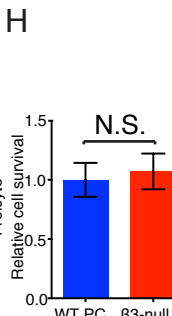
E



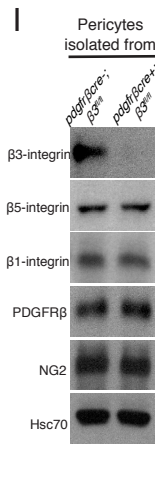
G



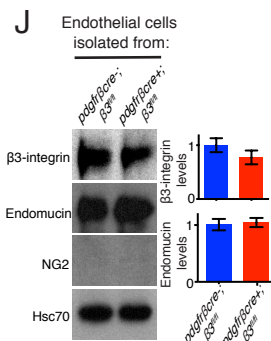
H



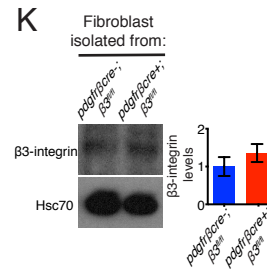
I



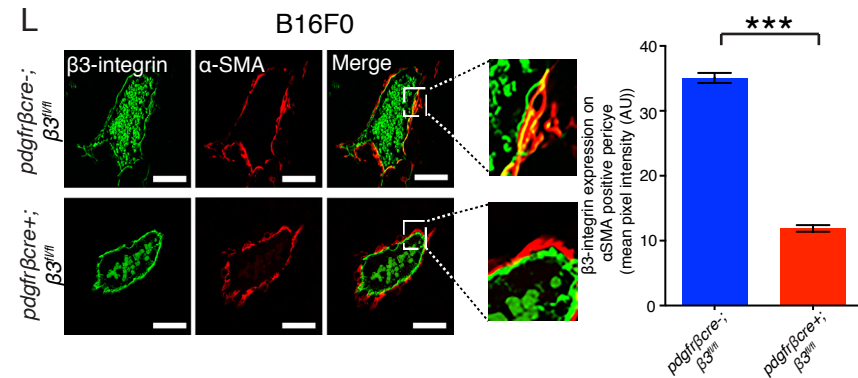
J



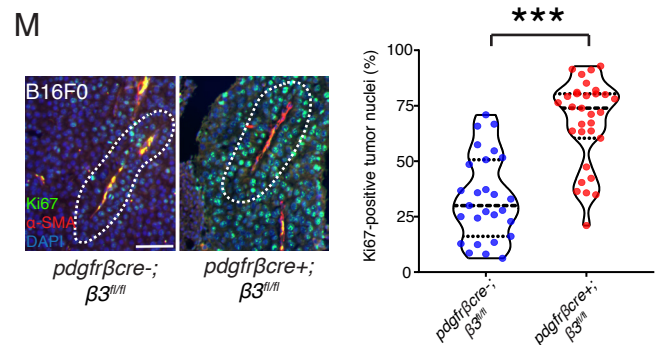
K



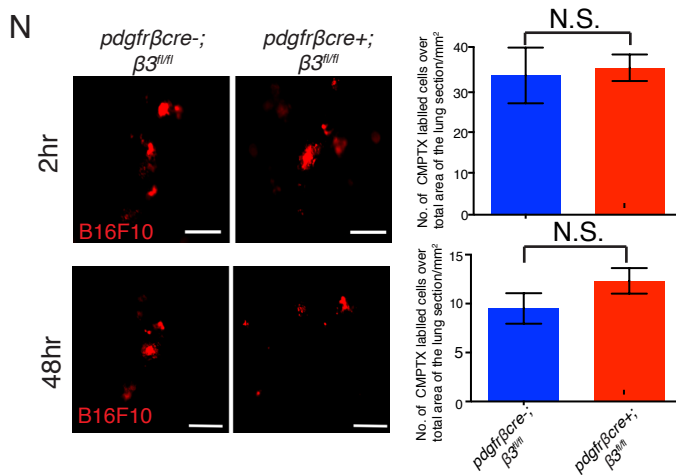
L



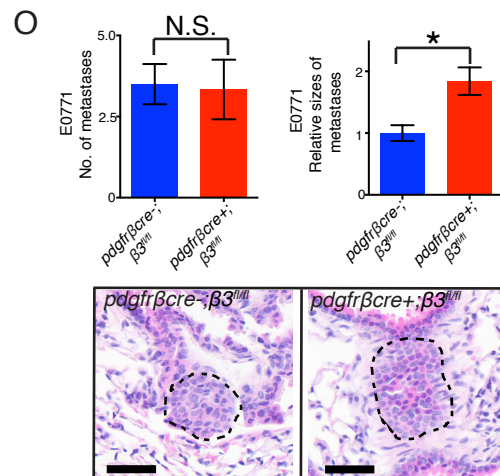
M

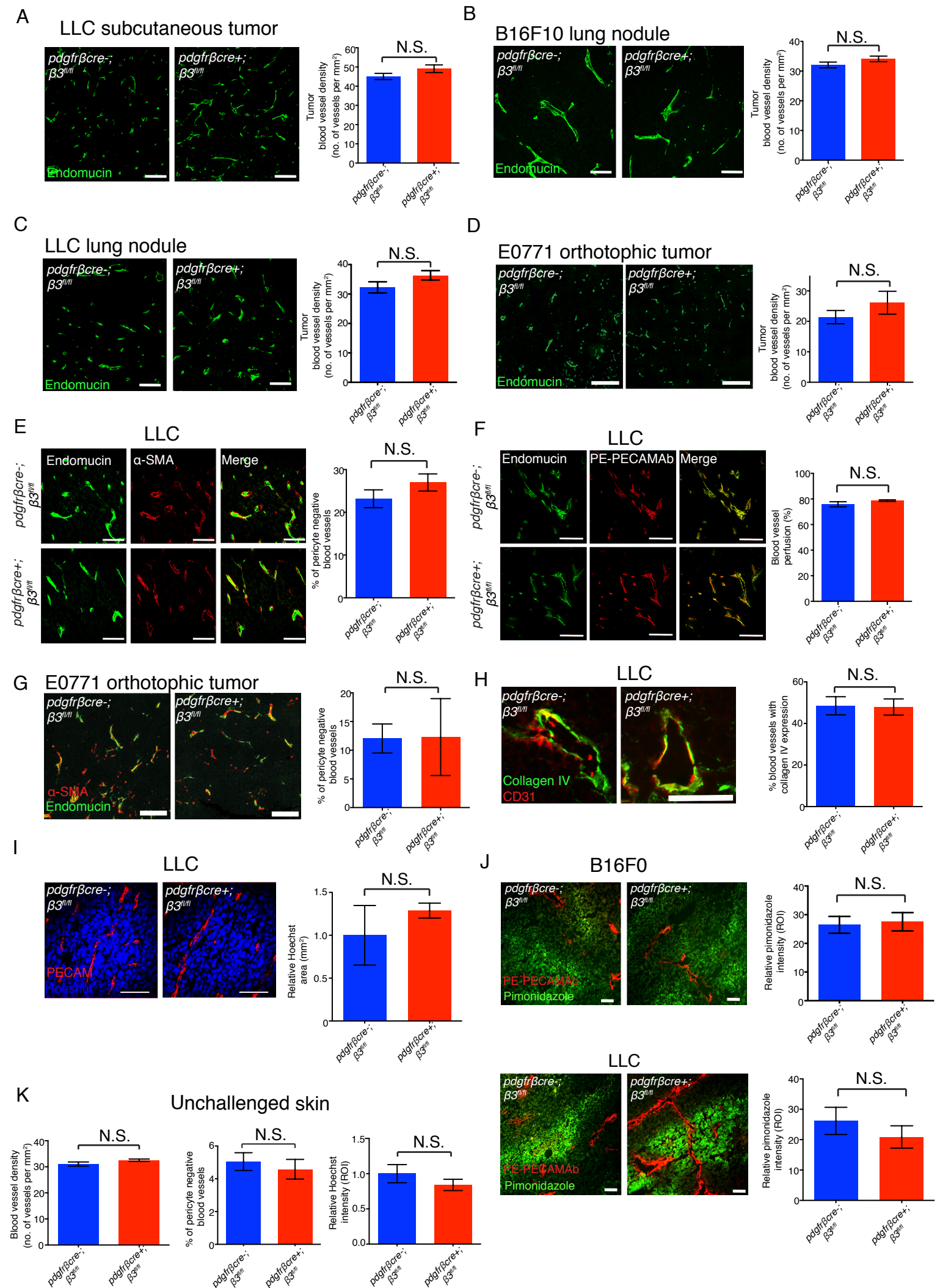


N

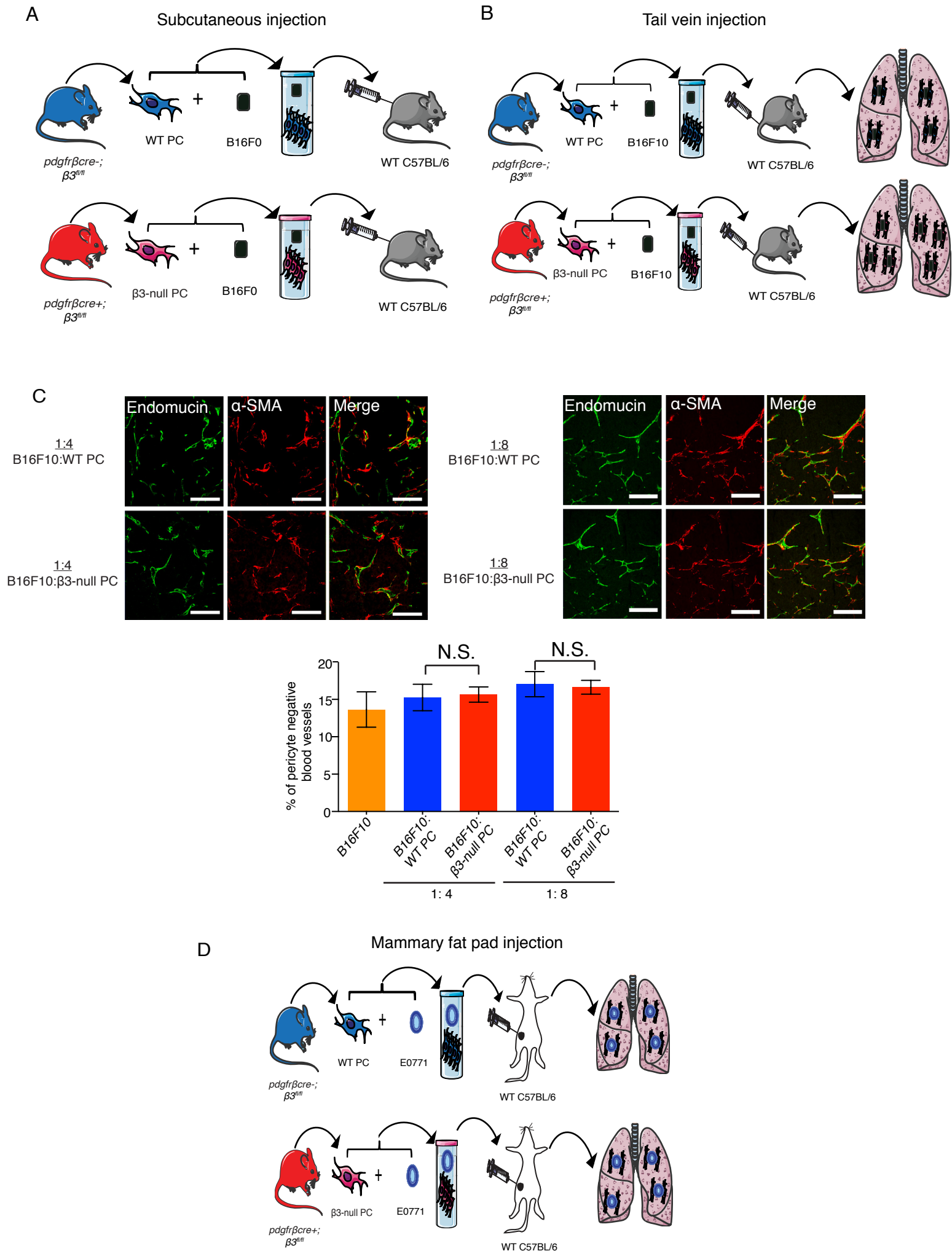


O

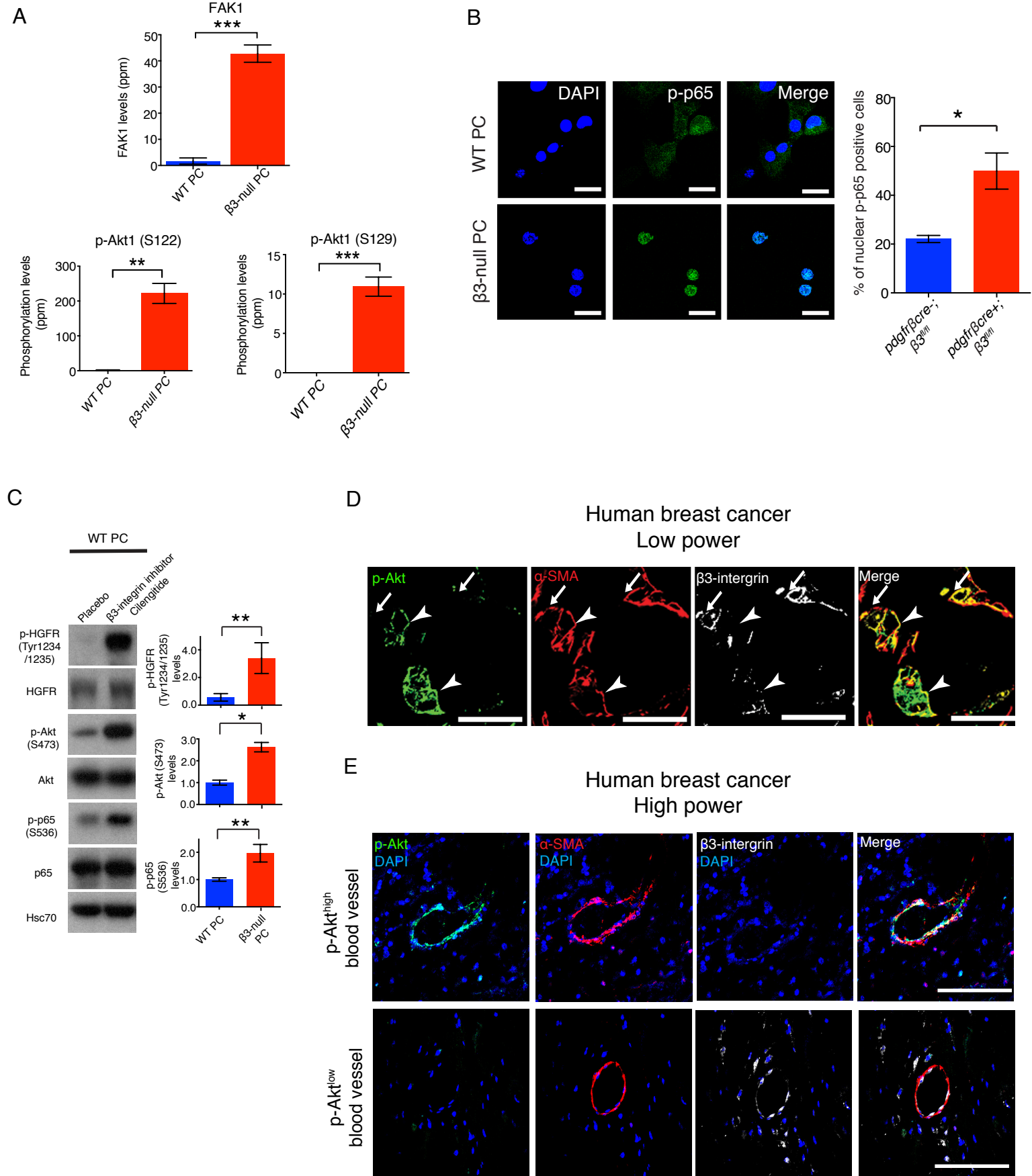




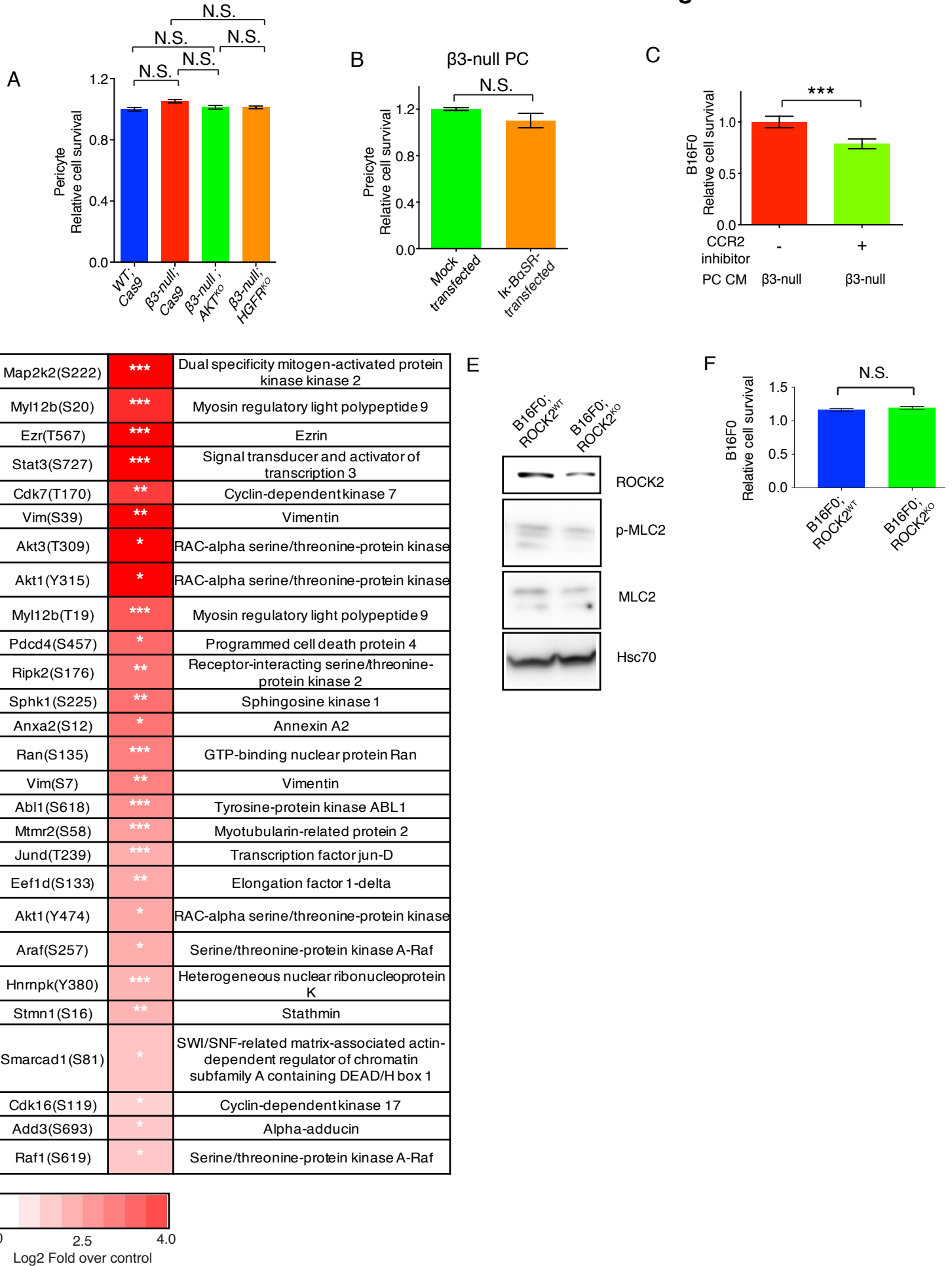
Wong, Muñoz-Félix *et al.*, Supplementary figure 4 related to figure 4



Wong, Muñoz-Félix *et al.*, Supplementary Figure 5
related to Figure 5



Wong, Muñoz-Félix *et al.*, Supplementary Figure 6 related to Figure 6 and 7



Code	Gene	Target sequence	Enrichment	Backbone
CGM48	mTIMP1	GAAACTCTTCACTGCGGTTC	FACS (EGFP)	PM1326, pLenti-CRISPR-EGFP (Addgene 75159)
CGM50	mCXCL1	ACTTCGGTTTGGGTGCAGTG	FACS (EGFP)	PM1326, pLenti-CRISPR-EGFP (Addgene 75159)
CGM52	mCCL2	GATGATCCCAATGAGTAGGC	FACS (EGFP)	PM1326, pLenti-CRISPR-EGFP (Addgene 75159)
CGM66	mAkt1	CATTGAGCGCACCTTCATG	FACS (EGFP)	PM1326, pLenti-CRISPR-EGFP (Addgene 75159)
CGM74	mHGFR	ATTCAAGACCGGGCCCGTGT	FACS (EGFP)	PM1326, pLenti-CRISPR-EGFP (Addgene 75159)
CGM74	mHGFR	ATTCAAGACCGGGCCCGTGT	FACS (EGFP)	PM1326, pLenti-CRISPR-EGFP (Addgene 75159)

Supplementary table 1. Construction of CRISPR/Cas9-EGFP plasmids. sgRNA sequences targeting TIMP1 (Gene ID: 21857), CXCL1 (Gene ID: 14825), CCL2 (Gene ID: 20296), Akt1 (Gene ID: 11651), and HGFR (Met) (Gene ID: 17295) (see table S1) were cloned into the pLenti-CRISPR–EGFP plasmid (Addgene-#75159) using BsmBI enzyme site.

Supplementary information

Supplementary Figure 1, related to main Figure 1. Representative images of mural $\beta 3$ -integrin negative and positive human tumor blood vessels. Representative images of double immunostained tumor sections for $\beta 3$ -integrin and α -SMA. Mural $\beta 3$ -integrin negative and $\beta 3$ -integrin positive vessels are given in melanoma (**A**), human lymphoma (**B**), human ER+ breast cancer (**C**) and mesothelioma (**D**). Yellow signal identifies $\beta 3$ -integrin and α -SMA co-staining. (**E**) In human melanoma, tumor cell proliferation is enhanced, indicating enhanced tumor growth, in patients where more than the mean (41) % of blood vessels are mural- $\beta 3$ -integrin negative. Scale bars (**A-D**) 10 μ m, (**E**) 50 μ m.

Supplementary Figure 2, related to main Figure 2. Characterization of $pdgfr\beta cre^{-};\beta 3^{fl/fl}$ and $pdgfr\beta cre^{+};\beta 3^{fl/fl}$ mice (**A**) Crossing $pdgfr\beta cre^{-};\beta 3^{fl/fl}$ and $pdgfr\beta cre^{+};\beta 3^{fl/fl}$ mice produced litters in which the numbers of $pdgfr\beta cre^{-};\beta 3^{fl/fl}$ and $pdgfr\beta cre^{+};\beta 3^{fl/fl}$ mice were born at predicted Mendelian ratios (n=95-100 mice per genotype). (**B**) Gender ratios of $pdgfr\beta cre^{+};\beta 3^{fl/fl}$ mice were normal (n=95-100 mice per genotype). (**C**) Mouse weights at 3 months old. No differences were observed in the weights of sex-matched mice between the two genotypes (n=25-28 mice per genotype). (**D**) All mice were analyzed by PCR genotyping. $\beta 3$ -integrin-floxed PCR identifying homozygous $\beta 3$ -integrin floxed ($\beta 3^{fl/fl}$) (270 bp), WT non-floxed ($\beta 3$ -integrin wt) (182 bp) and $pdgfr\beta cre$ PCR shows a product identifying $pdgfr\beta cre$ at 669 bp. (**E**) Representative H&E stained sections of heart, liver lung, kidney and spleen from 12 week old $pdgfr\beta cre^{-};\beta 3^{fl/fl}$ and $pdgfr\beta cre^{+};\beta 3^{fl/fl}$ mice. No gross morphological defects were observed. (**F**) *Upper panels*, Unchallenged adult skin from $pdgfr\beta cre^{-};TdTom$ immunostained for endomucin and PDGFR β shows weak PDGFR β expression in mural cells in 76.6% dermal vessels. No $TdTom$ signal was observed in $pdgfr\beta cre^{-};TdTom$ skin (data not shown). Unchallenged adult skin from $pdgfr\beta cre^{+};TdTom$ shows $TdTom$ reporter signal in only 32.6% of dermal blood vessels. Left panel, Arrows, PDGFR β -positive vessels, Arrowheads, PDGFR β -negative vessels. Right panel, Arrows, $TdTom$ -positive vessels, Arrowheads $TdTom$ -negative vessels. *Lower panels*, $pdgfr\beta cre^{-}$ and $pdgfr\beta cre^{+}$ mice were bred with $mTmG$ reporter mice, producing both $pdgfr\beta cre^{-};mTmG$ and $pdgfr\beta cre^{+};mTmG$ mice. B16F0s were subcutaneously inoculated into mice. Tumor blood vessels were examined for expression of both membrane-targeted tandem dimer Tomato (mT) (red), observed in host tissue, and membrane-targeted green fluorescent protein (GFP) (mG) (green), which is observed

only after Cre excision. GFP expression was found exclusively in mural cells surrounding blood vessels in *pdgfrβcre+;mTmG* mice only. **(G)** Flow cytometry of pericytes isolated from *pdgfrβcre-;β3^{fl/fl}* mice show that the purity of pericyte preparation is high. Pericyte preparations showed good expression of NG2, PDGFRβ and CD146 (all pericyte markers) and low levels of CD31 (endothelial cell marker), Mac1 (macrophage marker) and PDGFRα (fibroblast marker). Median values are given (n=3 experimental repeats). Negative controls (blue peaks), target signals (orange peaks). **(H)** MTS cell survival assay showing WT and β3-integrin-null pericytes relative cell survival. **(I)** Western blot analysis revealed that pericytes isolated from *pdgfrβcre-;β3^{fl/fl}* mice expressed β3-integrin whereas pericytes isolated from *pdgfrβcre+;β3^{fl/fl}* mice did not. Both genotypes expressed equal levels of β1-integrin, β5-integrin, PDGFRβ and NG2. Hsc70 acted as a loading control. Densitometric values are given (n=3 experimental repeats). **(J)** Endothelial cells isolated from *pdgfrβcre-;β3^{fl/fl}* and *pdgfrβcre+;β3^{fl/fl}* mice showed no deletion in β3-integrin, and expressed the endothelial marker endomucin but not the pericyte marker NG2 (n=3 experimental repeats). **(K)** Fibroblasts isolated from *pdgfrβcre-;β3^{fl/fl}* and *pdgfrβcre+;β3^{fl/fl}* mice also expressed β3-integrin. These data further support that loss of β3-integrin was not found in endothelial cells or fibroblasts but only in pericytes isolated from *pdgfrβcre+;β3^{fl/fl}* mice. Densitometric values are given. Results suggest that loss of β3-integrin is restricted to pericytes in *pdgfrβcre+;β3^{fl/fl}* mice. Bar charts represent means ± s.e.m. (n=3 experimental repeats). **(L)** Double immunofluorescence staining for β3-integrin and α-SMA demonstrated that pericytes in B16F0 subcutaneous tumors grown in *pdgfrβcre+;β3^{fl/fl}* mice had reduced β3-integrin expression levels. Magnified regions show β3-integrin-positive pericytes (yellow signal) on *pdgfrβcre-;β3^{fl/fl}* tumor blood vessels, but β3-integrin-negative pericytes on *pdgfrβcre+;β3^{fl/fl}* tumor blood vessels. Bar chart represents mean pixel intensity of β3-integrin expression in α-SMA positive cells ± s.e.m (n=5 tumors analyzed per genotype). **(M)** Ki67 endomucin double staining and Ki67 positive cell analysis in the perivascular areas (*dotted line*) of B16F0-tumors grown in *pdgfrβcre-;β3^{fl/fl}* mice and *pdgfrβcre+;β3^{fl/fl}* mice. Enhanced tumor cell proliferation in *pdgfrβcre+;β3^{fl/fl}* mice acts as an indicator of enhanced tumor growth. **(N)** *Pdgfrβcre-;β3^{fl/fl}* mice and *pdgfrβcre+;β3^{fl/fl}* mice were injected with 0.5 x 10⁶ CMTPIX labelled B16F10 melanoma cells via the tail vein. Mice were sacrificed and lungs harvested 2 and 48 hr after the injection. The number of CMTPIX positive cells in the lungs was not different between genotypes (n=9-10 lungs analyzed per group). **(O)** E0771 cells co-injected into the mammary fat pad in *pdgfrβcre-;β3^{fl/fl}* and *pdgfrβcre+;β3^{fl/fl}* mice, culled when tumors reached 600 mm³ and subsequent lung metastases assessed by analysis of

H&E stained sections. Results showed that although no changes in the numbers of metastases were observed, metastases were larger in *pdgfr β cre+; β 3^{fl/fl}* mice (N=8-9 mice per group). *p < 0.05, **p < 0.01, ***p<0.001. (C-O) Student's *t* test. Scale bar (E) 50 μ m, (F) 10 μ m, (L) 10 μ m, (M, O) 50 μ m, (N) 500 μ m,

Supplementary Figure 3, related to main Figure 3. Tumor blood vessel density, pericyte coverage and leakiness is not affected by pericyte- β 3-integrin-deletion. Sections of: (A) LLC subcutaneous, (B) B16F10 lung nodules, (C) LLC lung nodule and (D) E0771 orthotopic mammary tumors were stained for endomucin, and the number of vessels per mm² counted. Quantitation shows that the number of vessels per mm² was not affected in *pdgfr β cre+; β 3^{fl/fl}* mice. (E) Sections of LLC subcutaneous tumors were double immunostained for endomucin and α -SMA and the percentage of vessels with associated pericytes counted. Quantitation shows that the percentage of α -SMA-positive tumor blood vessels was not affected in *pdgfr β cre+; β 3^{fl/fl}* mice. (n=7-9 subcutaneous tumors analyzed per group). (F) Sections from subcutaneous LLC tumors from mice that had been injected via the tail vein with PE-PECAM ab (red), to detect perfused vessels, were immunostained for endomucin (green). Bar charts indicate that percentage of PE-PECAMab perfused endomucin-positive vessels. (G) Sections of E0771 orthotopic mammary tumors were double immunostained for endomucin and α -SMA and the percentage of vessels with associated pericytes counted. Quantitation shows that the percentage of α -SMA-positive tumor blood vessels was not affected in *pdgfr β cre+; β 3^{fl/fl}* mice. (n=7-9 subcutaneous tumors analyzed per group). (H) Sections from subcutaneous LLC tumors were double immunostained for basement membrane marker collagen IV (green) and CD31 as an endothelium marker (red). Bar charts indicate that the percentage of blood vessels with collagen IV expression in LLC tumor vascular basement membranes was unchanged between genotypes (n=9-10 tumors analyzed per group). (I) Relative area of perivascular Hoechst dye leakage (blue): PE-PECAM ab (red) in LLC tumors grown in *pdgfr β cre-; β 3^{fl/fl}* and *pdgfr β cre+; β 3^{fl/fl}* mice after ante-mortem intravenous injection of Hoechst dye. No significant change in perivascular leakage between *pdgfr β cre-; β 3^{fl/fl}* and *pdgfr β cre+; β 3^{fl/fl}* mice was observed. Bar charts represent means \pm s.e.m. (n=4-5 tumors analyzed per group). (J) Tumor hypoxia. Immunodetection of the hypoxia marker pimonidazole shows no significant difference between genotypes in tumor hypoxia in both B16F0 and LLC tumors grown in *pdgfr β cre-; β 3^{fl/fl}*

and *pdgfr β cre+; β 3^{fl/fl}* after ante-mortem administration of PE-PECAM ab to detect perfused vessels and pimonidazole to detect hypoxia. Bar charts represent means \pm s.e.m. (n=4-5 tumors analyzed per group). **(K)** Unchallenged skin from *pdgfr β cre-; β 3^{fl/fl}* and *pdgfr β cre+; β 3^{fl/fl}* mice were sectioned and double immunostained for endomucin and α -SMA. Quantitation of blood vessel density; pericyte association with blood vessels and vascular leakage, using Hoechst as above, was unchanged between genotypes. Bar charts represent means \pm s.e.m. (n=3-5 mice per group). N.S., no significant difference. **(A-K)** Student's *t* test. Scale bars in **(A-F)** 25 μ m, **(G, I, J)** 50 μ m, **(H)** 10 μ m.

Supplementary Figure 4, related to main Figure 4. β 3-integrin deficient pericytes enhance tumor cell growth independent of the tumor vasculature. Schematic representation of the protocol for co-injection of B16F0 tumor cells with WT or β 3-integrin null pericytes either **(A)** subcutaneously or **(B)** via the tail vein. **(C)** Immunofluorescence images of endomucin and α -SMA double immunostaining in sections of the lung nodules described in main Figure 4C. Quantitation shows no difference in blood vessel density or percentage of pericyte-free tumor blood vessels across any of the groups, demonstrating that elevated tumor growth in the presence of β 3-null pericytes is independent of blood vessel numbers and mural cell support. Bar charts represent means \pm s.e.m. (n=3-5) tumor burdened lungs analyzed per group. **(D)** Schematic representation of the protocol for the orthotopic co-injection of E0771 tumor cells and WT or β 3-integrin null pericytes into female C57BL/6 mice. N.S., no significant difference. PC, pericytes. N.S., no significant difference. **(C)** Student's *t* test. Scale bars in **(C)** 50 μ m.

Supplementary Figure 5, related to main Figure 5. Loss of β 3 expression or function enhances alternative signalling pathways. **(A)** Phosphoproteomic analysis identified levels of FAK1 and phosphorylated Akt1 (Ser122) and Akt1 (Ser129) in WT and β 3-integrin null pericytes. Bar charts represent ppm units of 3 different samples per group. **(B)** WT and β 3-null pericytes were immunostained for p-p65 and DAPI. Quantitation revealed that nuclear p-p65 was enhanced significantly in β 3-null pericytes. Bar charts represent means \pm s.e.m. (n=3 experimental repeats). **(C)** Western blot analysis of p-HGFR (Tyr1234/1235), HGFR, p-Akt (S473), total Akt, p-p65 (S536) and total p65 from WT pericytes treated with either placebo or the β 3-integrin inhibitor, cilengitide. Bar charts represent densitometric values \pm s.e.m (n=3 experimental repeats). Hsc70 acts as a loading control. **(D, E)** Triple

immunostaining of p-Akt, α -SMA and β 3-integrin in human breast cancer. Low power (**D**), and high power (**E**). α SMA positive mural cells with low p-AKT and high β 3-integrin or high p-AKT and low β 3-integrin. *p < 0.05, **p < 0.01, ***p < 0.001. (**A-C**) Student's *t* test. Scale bars in (**B, D**) 50 μ m, (**E**) 25 μ m.

Supplementary Figure 6, related to main Figures 6 and 7. Deletion of pericyte- β 3-integrin increases tumor cell growth via pericyte-CCL2 and tumor cell-MEK1 and ROCK2 pathways. (**A**) MTS assays showing no differences in cell survival between WT;Cas9, β 3-null;Cas9, β 3-null;Akt^{KO} and β 3-null;HGFR^{KO} pericytes (PC). (**B**) MTS assays showing no difference in cell survival between mock transfected and I κ -B α SR-transfected β 3-null pericytes. (**C**) MTS cell survival of B16F0 tumour cells treated with CM from β 3-null pericytes with vehicle or CCR2-inhibitor. (**D**) Phosphoproteomic analysis identifies enrichment of phosphorylated residues in B16F0 cells exposed to CM from β 3-null pericytes compared with WT pericytes. (**E**) Characterization of B16F0;ROCK2^{KO} cells. Western blot analysis of ROCK2, p-MLC2, MLC2 and Hsc70 used as loading control. (**F**) MTS assay shows no significant difference in cell survival between B16F0;ROCK^{WT} and B16F0;ROCK^{KO} cells. *p < 0.05, **p < 0.01, ***p < 0.001. N.S. No significant difference. (**A, B, C and F**) Student's *t* test.